Badlands: Basin & Landscape Dynamics

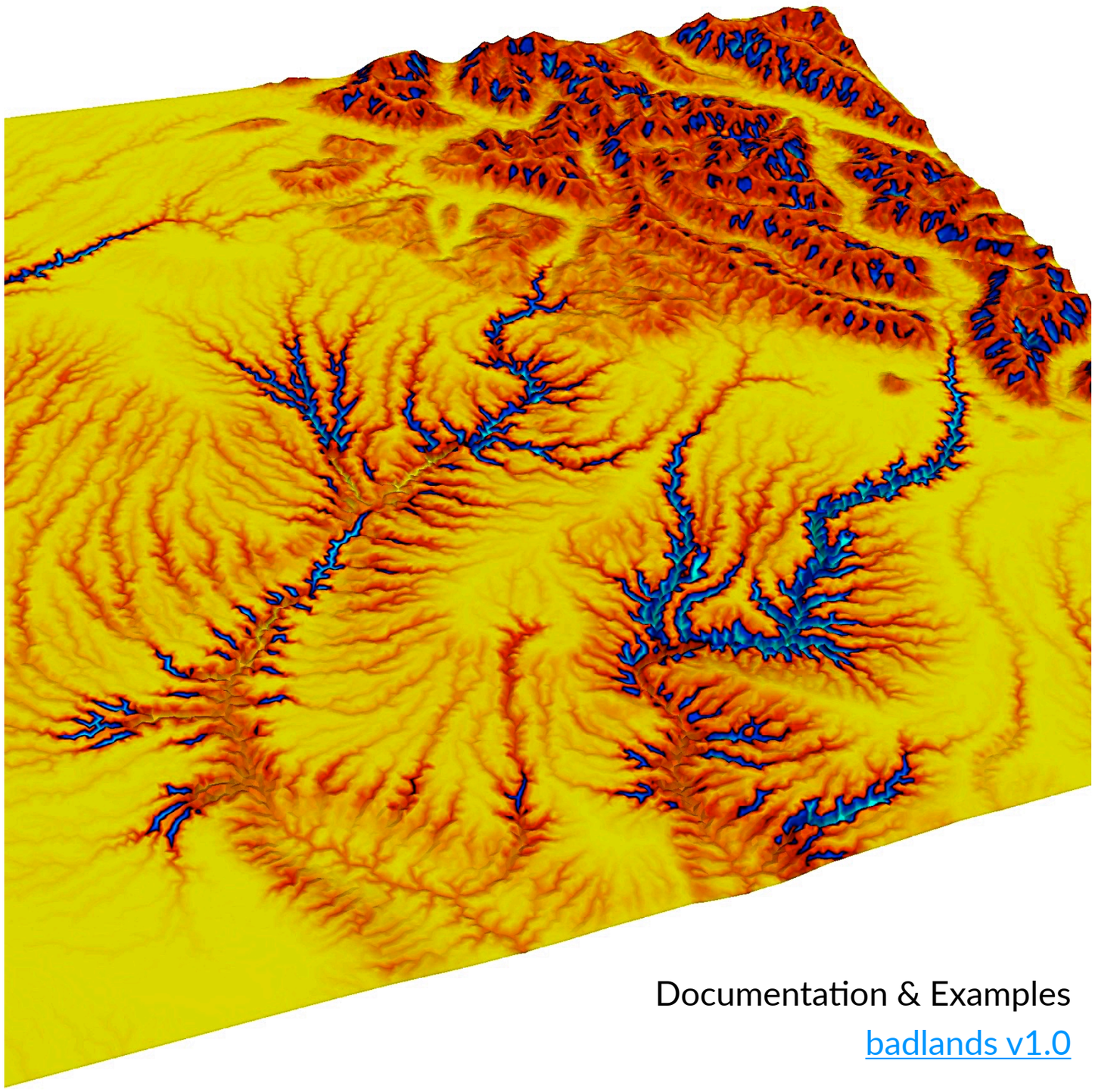

Documentation & Examples

badlands v1.0

CHAPTER 1

Equations for geomorphology

Overview of Badlands formulation

Peruvian landscape from the European Space Agency

SECTION 1

Landscape evolution models overview

The development of the **Badlands** model (**Ba**sin an**d** **lan**dscape **d**ynamic**s**) is made in the context of the growing number of landscape evolution models (or surface processes models - SPMs) that have been proposed during the last decades. Many geomorphological applications have demonstrated the usefulness of these models, whose predictions help researchers test simple to complex hypotheses on the nature of landscape evolution. SPMs also provide connection between small-scale, measurable processes and their long-term geomorphic implications (Tucker et al., 2001b). Below, we give a brief overview of SPMs, their history and their conceptual basis.

SURFACE PROCESSES MODELS

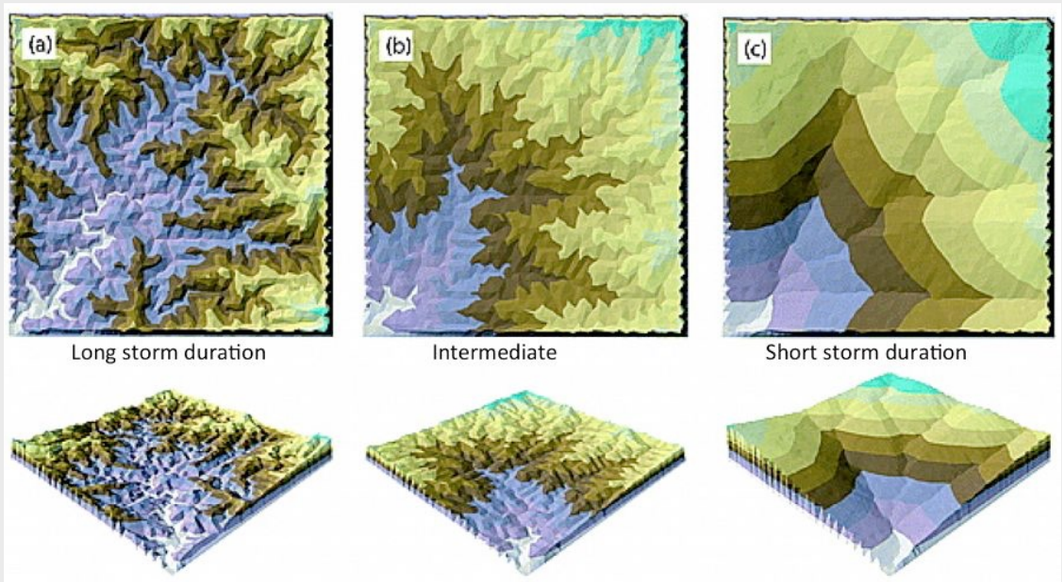

Role of storm duration in shaping catchment (Solyom & Tucker, 2004).

The roots of landscape evolution theory can be found in the pioneering work of Gilbert (1877), who proposed a set of hypotheses to relate various landforms to the mechanisms of weathering, erosion and sediment transport. The first quantitative models appeared later in the 1960s (*e.g.*, Culling, 1960; Scheidegger, 1961; Ahnert, 1970; Kirkby, 1971).

Models	Example reference	Note
SIBERIA	Willgoose et al. (1991)	Transport-limited; Channel activator function
DRAINAL	Beaumont et al. (1992)	“Undercapacity” concept
GILBERT	Chase (1992)	Precipiton
DELIM/MARSSIM	Howard (1994)	Detachment-limited; Nonlinear diffusion
GOLEM	Tucker & Slingerland (1994)	Regolith generation; Threshold landsliding
CASCADE	Braun & Sambridge (1997)	Irregular discretization
CAESAR	Coulthard et al. (1996)	Cellular automaton algorithm for 2D flow field
ZSCAPE	Densmore et al. (1998)	Stochastic bedrock landsliding algorithm
CHILD	Tucker & Bras (2000)	Stochastic rainfall
EROS	Crave & Davy (2001)	Modified precipiton
LAPSUS	Schoorl et al. (2002)	Multiple flow directions
APERO/CIDRE	Carretier & Lucazeau (2005)	Single or multiple flow directions
TISC	Garcia-Castellanos (2003)	Lithospheric-scale tectonics
FEM	Simpson & Schlunegger (2008)	Debris flow
FASTSCAPE	Braun & Willet (2013)	Implicit & parallel
LANDLAB	Tucker et al. (2014)	Python software package
CSDMS	http://csdms.colorado.edu/wiki/Main_Page	

These models formalize the concepts of Gilbert (1877) to the development of hillslope profiles. A few years later, these models were extended to two dimensions, although still focused on hillslope morphology (*e.g*, Ahnert, 1976; Kirkby, 1986). During the last two decades, as computers continued to get faster, a number of sophisticated numerical SPMs have been developed, mainly focusing on watershed or mountain belt evolution (*e.g.*, Willgoose et al., 1991; Howard, 1994; Braun and Sambridge, 1997; Densmore et al., 1998; Tucker et al., 2001b; Crave and Davy, 2001; Coulthard et al., 2002). Both hillslope and fluvial processes are involved in these models, which differ from each other by the parameterization of these processes and their numerical resolution. For a complete overview of surface processes modeling and the recent SPMs, the reader is referred to the numerous reviews on that topic (Beaumont et al., 1999; Coulthard, 2001; Martin and Church, 2004; Willgoose, 2005; Codilean et al., 2006; Bishop, 2007; Tucker and Hancock, 2010).

REFERENCES

Ahnert, F., 1970. A comparison of theoretical slope models with slopes in the field. Zeitschrift für Geomorphologie 9, 88–101.

Ahnert, F., 1976. Brief description of a comprehensive three-dimensional process-response model of landform development. Zeitschrift für Geomorphologie 25, 29–49.

Beaumont, C., Kooi, H., Willett, S., 1999. coupled tectonic-surface process models with applic- ations to rifted margins and collisional orogens. In: Summerfield, M. (Ed.), Geomorphology and Global Tectonics. Wiley, New York, pp. 29–55.

Bishop, P., 2007. Long-term landscape evolution: linking tectonics and surface processes. Earth Surface Processes and Landforms 32 (3), 329–365.

Braun, J., Sambridge, M., 1997. Modelling landscape evolution on geological time scales: a new method based on irregular spatial discretization. Basin Research 9 (1), 27–52.

Codilean, A., Bishop, P., Hoey, T. B., 2006. Surface process models and the links between tectonics and topography. Progress in Physical Geography 30 (3), 307.

Coulthard, T., 2001. Landscape evolution models: a software review. Hydrological Processes 15, 165–173.

Coulthard, T. J., Macklin, M. G., Kirkby, M. J., 2002. A cellular model of Holocene upland river basin and alluvial fan evolution. Earth Surface Processes and Landforms 27 (3), 269–288.

Crave, A., Davy, P., 2001. A stochastic “precipiton” model for simulating erosion/sedimentation dynamics. Computers and Geosciences 27 (7), 815–827.

Culling, W., 1960. Analytical theory of erosion. Journal of Geology 68, 336–344.

Densmore, A., Ellis, M., Anderson, R., 1998. Landsliding and the evolution of normal-fault-bounded mountains. Journal of Geophysical Research 103, 15203–15219.

Gilbert, G., 1877. Report on the Geology of the Henry Mountains. U.S. Geographical and Geo- logical Survey of the Rocky Mountain Region, Washington, D.C.

Kirkby, M. J., 1971. Hillslope process-response models based on the continuity equation. Inst. Brit. Geogr., Spec. Publ. 3, 15–30.

Kirkby, M., 1986. A two-dimensional simulation model for slope and stream evolution. In: Ab- rahams, A. (Ed.), Hillslope processes: Winchester, Mass. Allen and Unwin, pp. 203– 222.

Martin, Y., Church, M., 2004. Numerical modelling of landscape evolution: geomorphological perspectives. Progress in Physical Geography 28 (3), 317 – 339.

Scheidegger, A., 1961. Mathematical models of slope development. Geological Society of America Bulletin 72, 37–50.

Tucker, G. E., Hancock, G., 2010. Modelling landscape evolution. Earth Surface Processes and Landforms 35 (1), 28–50.

Tucker, G. E., Lancaster, S. T., Gasparini, N. M., Bras, R. L., Rybarczyk, S. M., 2001a. An object-oriented framework for distributed hydrologic and geomorphic modeling using triangulated irregular networks. Computers & Geosciences 27, 959–973.

Tucker, G. E., Lancaster, S. T., Gasparini, N. M., L, R., 2001b. The channel-hillslope integrated landscape development (CHILD) model. In: Harmon, R. S., Doe, W. (Eds.), Landscape Erosion and Evolution Modeling, iii Edition. Kluwer Academic/Plenum, New York, Ch. 12, pp. 349–388.

Willgoose, G., Bras, R. L., Rodriguez-Iturbe, I., 1991. A Coupled Channel Network Growth and Hillslope Evolution Model 1. Theory. Water Resources Research 27 (7), 1671–1684.

Willgoose, G., 2005. Mathematical Modeling of Whole Landscape Evolution. Annual Review of Earth and Planetary Sciences 33 (1), 443–459.

SECTION 2

Badlands: general equations

KEY POINTS

1. Continuity of mass.
2. Overland flow model.
3. Diffusion law for hillslope processes.
4. Flexural isostasy
5. Sediment compaction

CONTINUITY OF MASS

In the simplest case where there is no distinction between a regolith layer and the bedrock underneath, the mass continuity equations for a column of soil or rock is expressed as:

$$\frac{\partial z}{\partial t} = U - \nabla \cdot \mathbf{q}_s$$

where the elevation z (m) is measured vertically, $\mathbf{q}_s$ is the total downhill soil flux, $\nabla \cdot$ is the spatial divergence operator and U (m/yr) is a source term that can either represent the rate of incision of channel streams at the hillslope boundaries or uniform uplift. This is one of several variations; for discussion of others, see Tucker and Hancock (2010).

SEDIMENT TRANSPORT MODULES

To describe the rates of sediment erosion/transport/deposition, we use the following laws

OVERLAND FLOW: DETACHMENT-LIMITED MODEL

The soil transport rate per unit width by flowing water, $\mathbf{q_r}$, is modeled as a power function of topographic gradient ∇z and surface water discharge per unit width q_w (m^2/yr):

$$\mathbf{q_r} = -\kappa_r (q_w)^m (\nabla z)^n$$

Note that $(\nabla z)^n$ is short-hand for $\|\nabla z\|^{n-1} \nabla z$, as soil flux is oriented in the direction of the topographic gradient.

This detachment-limited incision rate, which is calculated as a power-law function of fluvial discharge only applies where channel slope is positive, (e.g., Howard, 1994; Whipple and Tucker, 1999):

$$\frac{\partial z}{\partial t} = -\kappa_r (q_w)^m (\nabla z)^n$$

This expression corresponds to a simplified form of the usual expression of sediment transport by water flow (Howard, 1980), in which the transport rate is assumed to be equal to the local carrying capacity, which is itself a function of boundary shear stress or stream power per unit width (Tucker and Hancock, 2010). We consider additionally no threshold for particle entrainment. The exponents m and n have values between 1 and 2 (Willgoose et al., 1991; Howard et al., 1994; Tucker and Bras, 1998; Prosser and Rustomji, 2000; Bogaart et al., 2003a).

Hillslope: Simple creep or linear diffusion

The parameterization of hillslope transport is based on a linear dependence to the topographic gradient. As pointed out by Fernandes & Dietrich (1997), this linear law has in fact been used to represent a variety of transport processes such as creep (*e.g.*, Culling, 1963; Armstrong, 1987), biogenic activity (*e.g.*, Dietrich et al., 1987; Heimsath et al., 1999, 2002) or rain splash (*e.g.*, De Ploey and Savat, 1968; Dunne et al., 2010). Downslope simple creep is commonly regarded as operating in a shallow superficial layer (Braun et al., 2001) and is defined as:

$$\mathbf{q_d} = -\kappa_d \nabla z$$

Note that because of the multi-process parameterization of soil transport, the coefficient κ_d is also scale-dependent (Dietrich et al., 1995), like the κ-scale parameters of the other transport laws included in our model.

Flexural isostasy

The equations governing elastic deformation are given by:

$$D \nabla^2 \nabla^2 w(x,y) = -(\rho_m - \rho_{fill}) g\, w(x,y) + q(x,y)$$

where D is the flexural rigidity of an elastic plate, $w(x,y)$ is the vertical deflection of the plate; ρ_m is the density of mantle; ρ_{fill} is the density of the material occupying the space created by the flexural subsidence (air/water/sediment). $q(x,y)$ is the net force per unit area exerted by the applied load,

$$q(x,y) = \rho_{load} g h_{load}(x,y)$$

ρ_{load} and h_{load} are the density and physical height of the load, respectively; g is the gravitational acceleration.

Various approaches to the numerical solution of the flexural deformation of an elastic plate have been described in the literature. Hodgetts et al. (1998) solved the 3D equation in the wave number domain via the 2D Fourier transforms. Another popular technique is to split the problem into two coupled Poisson equations for the deformation and the curvature (w and u). In **Badlands**, the adopted approach consists first in interpolating the load from the unstructured grid to an uniform one. Then 2 methods could be used by the user:

1. a 13-point second-order grid approximation,

2. a four-order multi-grid solutions to the biharmonic equation (Atlas et al., 1998).

The model is capable of simulating both local and regional isostatic compensation (Li et al., 2004).

Porosity and compaction

For basin-scale applications, compaction is an important phenomena which is the consequence of changes in sediment porosity due to overburden and pore fluid pressure. As for now **Badlands** only takes into account a unique time of sediment mixture and compaction during the

simulation is calculated using a *look-up table* containing porosity values as a function of effective stress. At given time interval and for each TIN node, the technique consists in

• iteratively computing the lithostatic pressure for all sedimentary time layers,

• deriving each sedimentary layer averaged porosity value from the *look-up table*.

• summing each layers compaction changes.

REFERENCES

Armstrong, A., 1987. Slopes, boundary conditions, and the development of convexo-concave forms—some numerical experiments. Earth Surface Processes and Landforms 12 (1), 17–30.

Altas, I., Dym, J., Gupta, M., Manohar, R.P., 1998. Multigrid solution of automatically generated high-order discretizations for the biharmonic equation. SIAM Journal on Scientific Computing 19, 1575–1585.

Bogaart, P. W., Tucker, G. E., Vries, J. J. D., 2003a. Channel network morphology and sediment dynamics under alternating periglacial and temperate regimes: a numerical simulation study. Geomorphology 54, 257 – 277.

Braun, J., Heimsath, A. M., Chappell, J., 2001. Sediment transport mechanisms on soil-mantled hillslopes. Geology 29 (8), 683–686.

Culling, W. E. H., 1963. Soil creep and the development of hillside slopes. The Journal of Geology 71 (2), 127–161.

Dietrich, W., Reneau, S., Reneau, C., 1987. Overview: 'Zero-Order Basins' and Problems of Drainage Density, Sediment Transport and Hillslope Morphology. In: Erosion and Sedimentation in the Pacific Rim. IAHS Publication No. 165. International Association of Hydrological Sciences, Washington, DC, pp. 27–37.

Dietrich, W. E., Reiss, R., Hsu, M. L., Montgomery, D. R., 1995. A process-based model for colluvial soil depth and shallow landsliding using digital elevation data. Hydrological Processes 9 (3-4), 383–400.

De Ploey, J., Savat, J., 1968. Contribution à l'étude de l'érosion par le splash. Zeitschrift für Geomorphologie 12, 174–193.

Dunne, T., Malmon, D. V., Mudd, S. M., Jan. 2010. A rain splash transport equation assimilating field and laboratory measurements. Journal of Geophysical Research 115 (F1), 1–16.

Fernandes, N., Dietrich, W. E., 1997. Hillslope evolution by diffusive processes: The timescale for equilibrium adjustments. Water Resources Research 33 (6), 1307–1318.

Heimsath, A., Dietrich, W. E., Nishiizumi, K., Finkel, R. C., 1999. Cosmogenic nuclides, topography, and the spatial variation of soil depth. Geomorphology 27, 151–172.

Heimsath, A. M., Chappell, J., Spooner, N. a., Questiaux, D. G., 2002. Creeping soil. Geology 30 (2), 111.

Hodgetts, D., Egan, S.S., Williams, G.D., 1998. Flexural modelling of continental lithosphere deformation: a com- parison of 2D and 3D techniques. Tectonophysics 294, 1–20.

Howard, A., 1980. Thresholds in river regimes. In: Coates, D. R., Vitek, J. D. (Eds.), Thresholds in Geomorphology. George Allen & Unwin, London, pp. 227–258.

Howard, A., 1994. A detachment limited model of drainage basin evolution. Water Resources Research 30, 2261–2285.

Li, F., Dyt, C., Griffiths, C., 2004. 3D modelling of the isostatic flexural deformation. Computer Geoscience 30, 1105–1115.

Prosser, I., Rustomji, P., 2000. Sediment transport capacity relations for overland flow. Progress in Physical Geography 24, 179–193.

Tucker, G. E., Bras, R. L., 1998. Hillslope processes, drainage density, and landscape morphology. Water Resources Reasearch 34 (10), 2751–2764.

Tucker, G. E., Hancock, G., 2010. Modelling landscape evolution. Earth Surface Processes and Landforms 35 (1), 28–50.

Whipple, K., Tucker, G., 1999. Dynamics of the stream-power river incision model: Implications for height limits of mountain ranges, landscape response timescales, and research needs. Journal of Geophysical Research 104 (B8), 17661–17.

Willgoose, G., Bras, R. L., Rodriguez-Iturbe, I., 1991. A Coupled Channel Network Growth and Hillslope Evolution Model 1. Theory. Water Resources Research 27 (7), 1671–1684.

Roering, J. J., 2008. How well can hillslope evolution models "explain" topography? Simulating soil transport and production with high-resolution topographic data. Geological Society of America Bulletin 120 (9), 1248.

Selby, M., 1993. Hillslope materials and processes, 2nd Edition. Oxford University Press.

Tucker, G. E., Bradley, D. N., Mar. 2010. Trouble with diffusion: Reassessing hillslope erosion laws with a particle-based model. Journal of Geophysical Research 115, 1–12.

Tucker, G. E., Bras, R. L., 1998. Hillslope processes, drainage density, and landscape morphology. Water Resources Reasearch 34 (10), 2751–2764.

Tucker, G. E., Hancock, G., 2010. Modelling landscape evolution. Earth Surface Processes and Landforms 35 (1), 28–50.

Whipple, K., Tucker, G., 1999. Dynamics of the stream-power river incision model: Implications for height limits of mountain ranges, landscape response timescales, and research needs. Journal of Geophysical Research 104 (B8), 17661–17.

Whipple, K., Tucker, G. E., 2002. Implications of sediment-flux-dependent river incision models for landscape evolution. Journal of Geophysical Research 107 (2039), 10–1029.

Willgoose, G., Bras, R. L., Rodriguez-Iturbe, I., 1991. A Coupled Channel Network Growth and Hillslope Evolution Model 1. Theory. Water Resources Research 27 (7), 1671–1684.

SECTION 3

Badlands: spatial and temporal framework

KEY POINTS

1. Spatial framework, finite volume approach.
2. Parallelization strategy.
3. Temporal framework.
4. 3D displacement: mesh geometry.

SPATIAL FRAMEWORK

Equations detailed in previous section describe the evolution of soil thickness and surface elevation. However, solving these partial differential equations (PDEs) is non-trivial and numerical methods are needed to perform their integration in space and time (for a given set of initial and boundary conditions). This step requires the discretization of the terrain surface, $z(x, y)$, and soil thickness, $h(x, y)$, into a finite number of 'hillslope elements', *i.e.*, a lattice of connected points (x_i, y_i) and their associated cells (*i.e.*, the part of the hillslope they represent) at which the solution of the PDEs is calculated. Here, we describe how the topography is discretized in **Badlands** and how the continuity of mass is applied within each element.

DELAUNAY TRIANGULATION AND VORONOI DIAGRAM

Here, we choose to use an irregular spatial discretization scheme similar to the CASCADE (Braun and Sambridge, 1997) and CHILD (Tucker et al., 2001a,b) models to numerically solve the geomorphic equations. The computational mesh is created in three stages: (1) The 2D planimetric space is first discretized as a set of points in any arbitrary configuration, (2) these points are then connected using the Delaunay triangulation (Voronoi, 1908; Delaunay, 1934) to form the nodes of a Triangulated Irregular Network (TIN), and (3) the Voronoi diagram, which corresponds to the dual graph of the Delaunay's TIN, is constructed. Initial values of surface elevation and soil thickness are then assigned to each node. These values will be updated every time step of a **Badlands** simulation.

The Delaunay triangulation and the Voronoi tessellation are well established in the field of computational geometry (*e.g.*, Fortune, 1992; Sambridge et al., 1995; Du, 1996). The Delaunay triangulation of a set of irregularly spaced points may be defined as the unique triangulation for

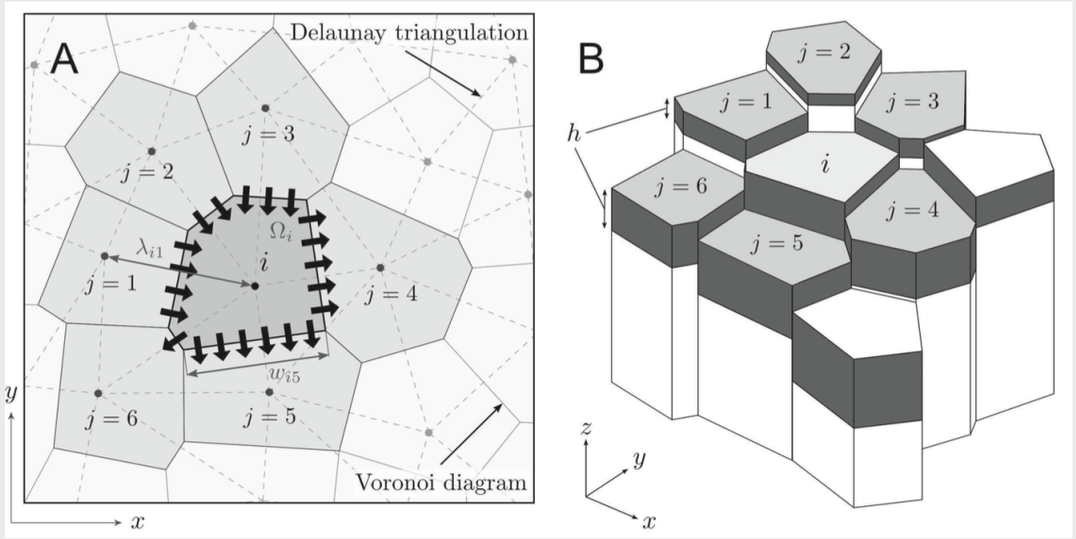

A mesh sample illustrating the discretization of the hillslope landscape in Badlands. A. Planimetric view showing the mesh nodes (points), the edges of the Delaunay triangles (dashed gray lines) connecting the nodes, and the edges of the corresponding Voronoi cells (plain lines). The thick arrows illustrate the fluxes - more precisely, their normal component - across the Voronoi polygon edges shared by the node i and its 'natural neighbours'. As examples, Ω_i is the area of the Voronoi cell of the node i; λ_{i1} is the planimetric distance between i and its 1st neighbour; and w_{i5} is the width of the Voronoi edge between the node i and its 5th neighbour (the order of the neighbours doesn't have any importance here). B. 3D representation of a subset of the Voronoi diagram showing the average elevation (height of the 'columns') and the average soil thickness (depth of the dark-gray volumes) associated to each Voronoi cell.

which the circles passing through the three vertices of each triangle do not contain any other node. Unlike other triangulation methods, this triangulation has the useful property of minimizing the maximum internal angles, thus providing the most 'equable' triangulation of the original set of points. In the Delaunay's TIN, each node is connected to a set of neighbours called the 'natural neighbours'. Its dual Voronoi diagram may be defined as the set of contiguous polygons (cells) formed by intersecting the perpendicular bisectors of the Delaunay triangles. The Voronoi cell about a node is the region of the plane that is closest to the node; it may be regarded as the 'neighbourhood' of the node. To build the mesh in **Badlands**, we use the Triangle implementation from Shewchuk of the Delaunay-Voronoi meshing algorithms.

Application of the finite-volume approach

As pointed out by Tucker et al. (2001b), the dual Delaunay-Voronoi framework lends itself to a numerical solution of the continuity equation using the Finite-Volume (FV) approach (Eymard et al., 2000). Applying this approach in our two-dimensional problem consists of integ- rating the continuity equation over small areas ('finite-volume' cells) surrounding the nodes of the mesh, which here correspond to the Voronoi cells associated to each node. Hereafter, we illustrate the application of the FV method to the node i and its associated Voronoi cell of surface area Ω_i. Using the divergence theorem, the integral over Ω_i of the divergence of the soil flux, $\nabla \cdot \mathbf{q_s}$, can be expressed as the integral of the soil fluxes at the boundary of the Voronoi cell:

$$\iint_{\Omega_i} \nabla \cdot \mathbf{q_s} d\Omega_i = \oint_{w_i} \hat{\mathbf{n}} \cdot \mathbf{q_s} dw_i \simeq \sum_{j=1}^{nb_i} w_{ij} q_{s,ij}$$

where w_i is the total length of the boundary of the Voronoi cell,$\hat{\mathbf{n}}$ is the unit vector normal to the boundary and pointing outward, nb_i is the number of natural neighbours connected to the node i, w_{ij} is the width of the edge shared by adjacent Voronoi cells associated to the node i and its neighbour j, and $q_{s,ij}$ is the total bulk volumetric soil flux across this edge per unit width.

The flux $q_{s,ij}$ is calculated by summing the fluxes defined in previous section, we note that this flux depends on the local topographic gradient across -and normal to- the shared Voronoi edge between the nodes i and j. This gradient is approximated as the topographic gradient between the nodes themselves:

$$\|(\nabla z)_{ij}\| \simeq S_{ij} = \frac{z_j - z_i}{\lambda_{ij}}$$

where z_i and z_j are the surface elevation associated to the nodes i and j , respectively, and λ_{ij} is the planimetric distance between these nodes. Considering the downslope movement of soil, $q_{s,ij}$ is positive if the net soil flux is from i to j, and negative if the net flux is from j to i. Note also that FV methods are conservative, *i.e.*, that the flux entering (or leaving) a given cell equals the flux leaving (or entering) the adjacent cell ($q_{s,ij} = -q_{s,ji}$). Finally, integrating both sides of the continuity equation over Ω_i gives:

$$\frac{dh_i}{dt} = \kappa P_{s,i} - \frac{1}{\Omega_i}\left(\sum_{j=1}^{nb_i} w_{ij} q_{s,ij}\right)$$

Intuitively, this equation simply states that a non-zero net soil flux out of the Voronoi cell surrounding the node i would result in a general decrease of soil thickness within this cell if the net flux is not balanced by the rate of soil production (inversely, a non-zero net flux entering the cell will always result in accumulation of soil within the cell). Note that in FV applications, the cells -and not the nodes of the mesh- are the primitive elements of the spatial discretization. Because the soil fluxes acting inside the cells are not considered, by using the divergence theorem it is only possible to describe the average rate of soil removal or accumulation, dh/dt, within each cell. When mentioning values of soil thickness, h_i, and surface elevation, z_i , assigned to the node i, we thus refer to the averages over the corresponding Voronoi cell.

Nodes ordering

Key to the model is to find the order in which one must go through the nodes to compute discharge by adding progressively the contribution of each node to the river discharge (or its contributing area to the total drainage area). To perform this operation, we assume that water goes down the path of the steepest slope (O'Callaghan and Mark, 1984; Gallant and Wilson, 2000). Our algorithm is thus based on the single-flow-direction approximation (each node has a single receiver) (O'Callaghan and Mark, 1984).

The approach we used is based on the work from Braun & Willett (2013) who presented a algorithm to solve very efficiently the stream power equation, regardless of problem geometry or boundary conditions. Its main advantages are that the computational time is linearly dependent on the number of nodes used to discretize the landform.

Parallelization Approach

To increase the model's computational efficiency, a two-level mapping parallelism technique is employed.

The first level of parallelism handles the mesh partitioning. Features and functions directly related to the mesh and its geometry are resolved and stored on each partition.
The second level of parallelism is specifically designed to efficiently compute stream network dynamics.

Mesh partitioning

At the beginning of a simulation, surface nodes positions representing initial are known. Once the irregular surface has been generated, the set of nodes is partitioned into subdomains. Each subdomain can then be mapped onto a processor of a parallel architecture. For our purposes, we consider a mesh partitioner desirable if it produces subdomains of nearly equal size (where size is measured by number of nodes) and with as few nodes shared between processors (ghost nodes) as is reasonably possible. The model partitioner uses the Hilbert Space-Filling Curve method algorithm, a description of the method is found in Zoltan library (Catalyurek et al., 2007; Devine et al., 2009).

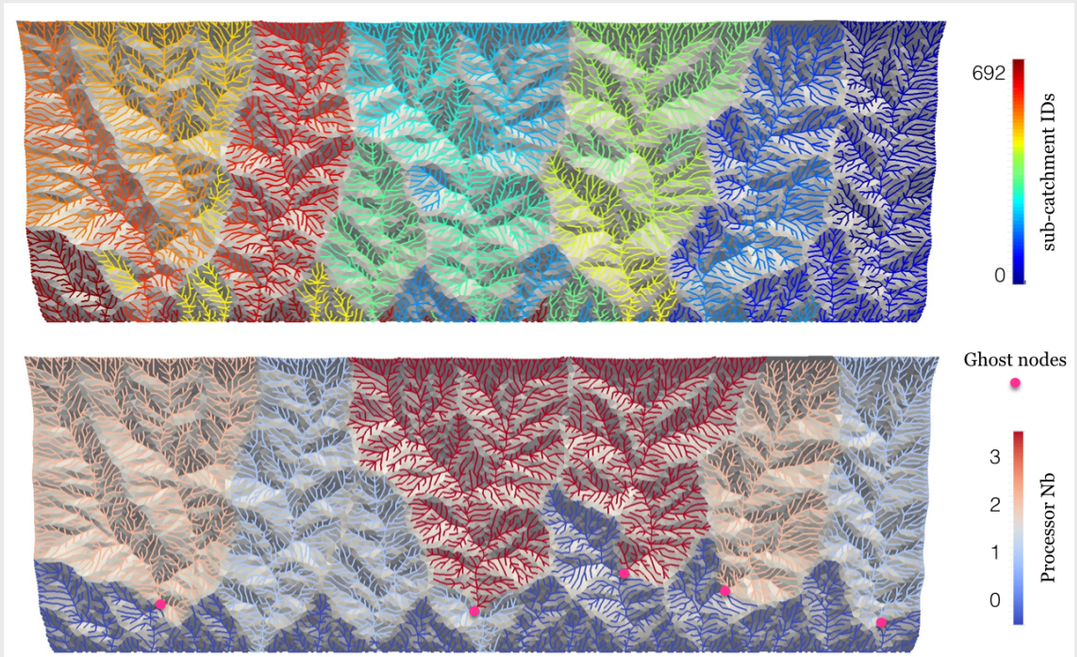

Stream network partitioning strategy. First the drainage is divided in several sub-basins (top figure). Then the partitioning approach consists in (1) minimizing the number of communication points (ghost cells) and (2) splitting the work load (number of nodes) uniformly between processors (bottom figure).

Stream network partitioning

The channel network is used as an acyclic, directed graph, such that reaches and junctions are ordered from upstream to downstream direction. Individual sub-basins draining to channel reaches form the basis for partitioning a large domain into smaller units and synchronizing effort in an upstream to downstream order.

The basic tradeoff in the parallelization of the model is determining how much computational effort occurs in a single sub-basin *vs.* the amount of message passing required between sub-basins. The computational effort in a sub-basin is determined by the number of nodes retained in the TIN and the sub-basin size. Data exchanges between sub-basins consist of lateral surface fluxes through the channel network in upstream to downstream order. Exchanges are performed through message passing using "ghost" cells, which are located at junctions between sub-catchments.

The variables exchanged through ghost cells occur within a model time step according to the sequential order of the processes and the upstream to downstream arrangement of domain nodes. Thus, the computations are synchronized by the structure of the interconnected system of basin nodes. The ghost cells receive, store and send the variables across the TIN nodes when these are located on separate processors.

Sub-basin (or graph) partitioning is generated through the graph partitioning code METIS (Karypis and Kumar, 1999). This approach is based on adjacency in the ordered flow network instead of geo-graphical proximity. The partitioning balances the number of TIN nodes across processors and minimizes the dissections that occur in the channel network through surface ghost cells.

Temporal framework

In **Badlands**, the time evolution of soil thickness and surface elevation is treated explicitly, *i.e.*, the values at the beginning of the next time step are fully determined by the values at the beginning of the 'current' time step. The time integration of the continuity equations gives:

$$
\begin{aligned}
h_i(t+\Delta t) &= h_i(t) + \frac{dh_i}{dt}\Delta t \\
z_i(t+\Delta t) &= z_i(t) + \left(\frac{dh_i}{dt} - \kappa P_{s,i} + U\right)\Delta t
\end{aligned}
$$

where Δt is the duration of the time steps, and where the values of $P_{s,i}$, U and all time-dependent variables used to calculate dh_i/dt (*i.e.*, the variables involved in the expressions of the soil fluxes) are those at the beginning of the current time step.

Using an explicit time integration scheme, the length of the time steps must be less than a certain time to ensure numerical stability (*i.e.*, to avoid any exponential magnification of approximation errors or numerical artifacts as the simulation proceeds).

CFL-LIKE CONDITIONING

At the beginning of each iteration, the maximal time step is calculated for the adopted first-order, forward-in-time scheme, and is chosen by calculating the minimum CFL factor for the simulated surface processes.

For the simple creep, the CFL factor takes the form:

$$\Delta t_{max} < min_{ij} \left(\frac{\lambda_{ij}^2}{2\kappa_d} \right)$$

The determination of the CFL limit for the nonlinear diffusion equation is quite tricky (see *e.g.* Pelletier, 2008; Press et al., 1992). We calculate an approximate limit as:

$$\Delta t_{max} \ll min_{ij} \left(\frac{\lambda_{ij}^2 - \frac{|z_j - z_i|}{S_c^2}}{2\kappa_{nd}} \right)$$

where the inequality is forced by multiplying the right-hand side by a factor such as 0.1 or less. The last expression must be evaluated at each iteration, since it depends on the surface slopes.

For the detachment-limited transport law the CFL upper limit for a given time step is given by:

$$\Delta t_{max} < min_{ij} \left(\frac{\lambda_{ij}}{\kappa_r q_{w,i}^m \left(\frac{|z_i - z_j|}{\lambda_{ij}} \right)^{n-1}} \right)$$

These CFL conditions serve as initial estimates of required time step but we apply an additional constraint detailed below to ensure numerical stability.

ADJUSTMENT OF SOIL TRANSPORT FLUXES

A straightforward application of the time integration of the continuity equations would lead to incorrect or undesirable results. The main reason is that even with small, though reasonable, time steps, numerical instability may be locally initiated by too-rapid removal or accumulation of soil. To ensure that this undesirable effect never occurs during a simulation, we assume that the amount of soil leaving a cell cannot produce a lowering of surface elevation greater than the difference - multiplied by a factor α (< 1) - of elevation between the cell and its downslope adjacent cell (receiver z_r). And that the amount of deposition inside a given cell cannot be higher than the difference - multiplied by α - of elevation between the cell and the lowest upstream adjacent node z_m. Because diffusive processes tend to smooth out the roughness of the terrain surface, they are not favorable to the initiation of numerical instability. In fact, the addition of a maximum threshold of elevation lowering is only imposed by the action of transport by overland flow. The restrictions described above can be expressed as the following set of inequalities:

$$\begin{aligned} \frac{\Delta t}{\Omega_i} \left(\sum_j w_{ij} q_{s,ij}^{in} - \sum_j w_{ij} q_{s,ij}^{out} \right) &\leq \alpha (z_r - z_i), \quad \sum_j w_{ij} q_{s,ij}^{out} > \sum_j w_{ij} q_{s,ij}^{in} \\ &\leq \alpha (z_m - z_i), \quad \sum_j w_{ij} q_{s,ij}^{in} > \sum_j w_{ij} q_{s,ij}^{out} \end{aligned}$$

where $q_{s,ij}^{out}$ is the flux of soil leaving the Voronoi cell of the node i, $q_{s,ij}^{in}$ the fluxes of soil coming from the adjacent cells.
To meet these restrictions for any amount of available soil and/or soil fluxes of any magnitude, a solution consists in choosing the minimal time step Δt which satisfies this set of inequalities.

DEFORMING MESH UNDER 3D DISPLACEMENTS

Due to tectonic advection, the density of surface nodes evolves over time, which leads to areas showing rarefaction or accumulation of nodes. In order for the interpolation schemes (based on local methods) to remain accurate and to avoid unnecessary computations, a local addition and deletion of nodes and the consequent remeshing of the triangulated surface are therefore required. The deletion, addition, and triangulation of nodes are performed at given time generally coincident with the coupling time with a geodynamics model (Underworld).

While the **Badlands** surface is required to be an irregular mesh to avoid potential directional bias of water flow (Braun & Sambridge, 1997), too irregular a mesh is not appropriate. The Triangle library is used to produce constrained Delaunay and to limit the creation of too irregular grids. For each newly advected TIN surface, **Badlands** algorithm ensures that the new nodal distribution

1. prevents the occurrence of low node density areas, and

2. enforces the required resolution for surface processes.

In addition, a node deletion/merging algorithm has been implemented to circumvent the problem of progressive increase of node number density (for example at mountain fronts) which could lead to significant slowdown of the surface process model.

REFERENCES

Braun, J., Sambridge, M., 1997. Modelling landscape evolution on geological time scales: a new method based on irregular spatial discretization. Basin Research 9 (1), 27–52.

Braun, J. and Willett, S.D., 2013. A very efficient, O(n), implicit and parallel method to solve the basic stream power law equation governing fluvial incision and landscape evolution. Geomorphology, v.180-181, 170-179.

Catalyurek, U., E., Boman, K., Devine, D., Bozdag, R., Heaphy, and L., Riesen (2007), Hypergraph-based dynamic load balancing for adaptive scientific compu- tations. IEEE In: Proc. of 21st International Parallel and Distributed Processing Symposium (IPDPS'07).

Delaunay, B., 1934. Sur la sphère vide. Akademii Nauk SSSR, Otdelenie Matematicheskikh i Estestvennykh Nauk 7, 793–800.

Devine, K., E., Boman, L., Riesen, U., Catalyurek, and C., Chevalier (2009). Getting started with zoltan: A short tutorial. In: Proceedings of 2009 Dagstuhl Seminar on Combinatorial Scientific Computing.

Du, C., 1996. An algorithm for automatic Delaunay triangulation of arbitrary planar domains. Advances in Engineering Software 27, 21–26.

Eymard, R., Gallouët, T., Herbin, R., 2000. Finite Volume Methods. In: Ciarlet, P., Lions, J. (Eds.), Handbook of Numerical Analysis, Vol. VII. Vol. M. North Holland, Amsterdam, pp. 713–1020.

Fortune, S., 1992. Voronoi diagrams and Delaunay triangulations. In: Du, D., Hwang, F. (Eds.), Computing in Euclidian Geometry. World Scientific, pp. 193–233.

Gallant, J., Wilson, J., 2000. Primary terrain attributes. In: Wilson, J., Gallant, J. (Eds.), Terrain Analysis: Principles and Applications. John Wiley and Sons, New York, pp. 51–85.

Karypis, G., Kumar, V., 1999. A fast and high quality multilevel scheme for partitioning irregular graphs. SIAM J. Scientific Comput. 20 (1), 359–392.

O'Callaghan, J., Mark, D., 1984. The extraction of drainage networks from digital elevation data. Computer Vision, Graphics, and Image Processing 28, 323–344.

Sambridge, M., Braun, J., McQueen, H., 1995. Geophysical parametrization and interpolation of irregular data using natural neighbours. Geophysical Journal International 122 (3), 837–857.

Tucker, G. E., Lancaster, S. T., Gasparini, N. M., Bras, R. L., Rybarczyk, S. M., 2001a. An object-oriented framework for distributed hydrologic and geomorphic modeling using triangulated irregular networks. Computers & Geosciences 27, 959–973.

Tucker, G. E., Lancaster, S. T., Gasparini, N. M., L, R., 2001b. The channel-hillslope integrated landscape development (CHILD) model. In: Harmon, R. S., Doe, W. (Eds.), Landscape Erosion and Evolution Modeling, iii Edition. Kluwer Academic/Plenum, New York, Ch. 12, pp. 349–388.

Voronoi, G., 1908. Nouvelles applications des paramètres continus à la théorie de formes quadratiques. Journal für die reine und angewandte Mathematik 134, 198–287.

CHAPTER 2

Badlands install & quick start

Badlands source code is available from GitHub
badlands v1.0

Photography by Adriana Franco, National Geographic

SECTION 1

Badlands: installation & dependencies

KEY POINTS

1. Instruction for installation.
2. Dependencies.
3. Compilation.

DEPENDENCIES

This section provides steps and links on obtaining and setting up **Badlands** model. The following instructions assume a beginner's level of familiarity with the Unix/Linux operating environment, including:

- *How to open a terminal window,*
- *How to navigate between directories using a terminal application,*
- *How to open, edit, save and close a file using an editor through a terminal application.*

Badlands relies on a suite of software applications, which need to be installed prior to compiling the code. It is recommended that you install each program in the order listed.

COMPILERS

Badlands is currently supported for GNU compilers , however it works as well with Intel compilers. Both C and fortran compilers are required.

For Linux OS , they should already been installed with your distribution. GNU compilers for Mac OS can be downloaded from the HPC website.

To install them you could follow the explanations provided on the website or proceed as follow in a Terminal:

```
$ gunzip gcc-X.X-bin.tar.gz
$ sudo tar -xvf gcc-X.X-bin.tar -C /
```

It installs everything in **/usr/local**. Then edit your **~/.profile** or **~/.bashrc** and set up the path to the installed compilers.

```
export PATH=/usr/local/bin:$PATH
export LD_LIBRARY_PATH=/usr/local/lib:$LD_LIBRARY_PATH
```

Now update the configuration file in your Terminal by typing:

$ source ~/.profile or **~/.bashrc**

Message Passing Interface

Badlands supports **MPICH** and **OpenMPI**. Below you will find guide to install **MPICH**. **MPICH** can be downloaded from the here. You will need to download the source code such as the **mpich-3.1** (stable release).

Once downloaded, open a Terminal, go to the **untar** folder and do:

$ tar -xvf mpich3-xxx.tar
$ cd mpich3-xxx
$ CC=gcc FC=gfortran CXX=g++ ./configure --prefix=/usr/local/mpich --enable-fast=all --enable-shared --enable-sharedlibs=osx-gcc
$ make
$ sudo make install

Then edit your **~/.profile** or **~/.bashrc** and set up the path to the installed compilers.

export MPI_DIR=/usr/local/mpich
export PATH=$MPI_DIR/bin:$PATH
export LD_LIBRARY_PATH= $MPI_DIR/lib:$LD_LIBRARY_PATH

Now update the configuration file in your Terminal by typing:

$ source ~/.profile or **~/.bashrc**

HDF5

HDF5 can be downloaded from the Hdf5 website. You will need to download the source code available for all platform such as the **HDF5-1.8.13** release. Once downloaded, open a Terminal and navigate to he **untar** folder and do:

$ CC=mpicc FC=mpif90 ./configure --prefix=/usr/local/hdf5 --enable-parallel --enable-fortran

After the configuration script has finished, checked the summary of the log which is printed on your screen and ensure that both **HDF5** for Fortran and C are present as well as the **HDF5** compression facility (**zlib**). If **zlib** is missing you will have to install it first following documentation in the zlib website.

$ make
$ sudo make install

XML Parser

FoX XmL can be downloaded from there. You will need to download the source code available as a tarball such as **FoX=4.1.2.tar.gz**. Once downloaded, open a Terminal and navigate to the **untar** folder and do:

$ cd FoX-xxx
$ FCFLAGS='-O2 -fPIC' FC=mpif90 ./configure --prefix=/usr/local/FoX
$ make
$ sudo make install

Once compiled, you will need to open the **/usr/local/FoX/bin/FoX-config** file using your preferred editing file:

$ sudo emacs /usr/local/FoX/bin/FoX-config

And change the **comp_prefix** (third line of the file) to the correct prefix in this case: **/usr/local/FoX** and delete the **/objs** at the end of the path.

Metis

The Metis library is available from there. Once downloaded, open a Terminal and navigate to the **untar** folder and do:

$ cd metis-xxx
$ make config cc=mpicc prefix=/usr/local/metis
$ sudo make install

Zoltan

Zoltan needs to be downloaded from Sandia website. Once downloaded, open a Terminal and create a building folder:

```
$ mkdir zoltanbuild
$ cd zoltanbuild
$ ../Zoltan_v3.81/configure --enable-f90interface --enable-mpi --with-mpi-compilers --with-gnumake --prefix=/usr/local/zoltan
$ make everything
$ sudo make install
```

Fire-up Badlands

Badlands can be cloned from GitHub.

```
$ git clone git://github.com/badlands-model/Badlands.git
```

Please always refer to the above site for latest software updates. Prior to starting the compilation process, you will need to check the path to the libraries you've installed on your system as they might differ from one to the other. In Badlands, the configuration are set in the **config** folder. The folder contains several files associated to different environments *e.g.* Linux/Mac or Intel/Gnu. Depending on the ones you've installed, copy the corresponding file and edit it:

```
$ cp Makefile.cfg.osx Makefile.cfg.myconfig
$ emacs Makefile.cfg.myconfig
```

In the file, check that the paths are set correctly. If not sure look at your **~/.profile** or **~/.bashrc**. Make the necessary changes and save your file. Now open the **Makefile.inc** file and change the first line to match with your new configuration file name:

```
CFGFILE = $(TOP)/config/Makefile.cfg.myconfig
```

Then compile Badlands sources from the top directory:

```
$ make clobber
$ make dist
```

SECTION 2

Badlands: input files

KEY POINTS

1. General parameters.
2. Forcing parameters.
3. Processes parameters.

Badlands is using **XML** input file. External **ASCII** files are referenced inside the **XML** document and provide information on the basal node position, the changes in forcing parameters, *e.g.* uplift/subsidence, rainfall and sea level.

To start with a working **XML** input file it is recommended to use one of the examples provided in the next chapter.

GENERAL PARAMETERS

GEOMETRY

<struct_geometry>

The first structure which appears in the input file is related to the definition of the geometry: initial surface (regular grid) & triangular irregular network (**TIN**) parametrization.

<regular_grid>

refers to the name of the regular surface nodes file **ASCII** and its path. The path is from the main input file location. The file provides for each line the following information:

- X coordinates in meters (this axis has a West to East orientation),
- Y coordinates in meters (this axis has a South to West orientation), &
- Z coordinates in meters.

Nodes must be defined in increasing order from the South/West corner, first along the X axis.

<delaunay_area>

sets a maximum area constraint when generating the Delaunay triangulation. No triangle will be generated whose area is larger than that number. This area should be the at least equal to a regular grid cell area.

<delaunay_angle>

sets a minimum angle constraint when generating the Delaunay triangulation. If the minimum angle is 20.7° or smaller, the triangulation algorithm is theoretically guaranteed to terminate. In practice, the algorithm often succeeds for minimum angles up to 33°. It usually doesn't terminate for angles above 34°.

<refine_area>

defines the number of high resolution areas in the simulation.

Note: the number of refine_area in v1.0 is limited to 1.

<ra>

initial entry class to set the properties of a specific high resolution area. A high resolution area is defined as a squared box which extends have to be defined within the simulated area and be at least two regular grid cells inside the domain. If the refine_area is set to 0 this **XML** component is not required.

- **<xmin>** SW X corner of the considered high resolution area,
- **<ymin>** SW Y corner of the considered high resolution area,
- **<xmax>** NE X corner of the considered high resolution area,
- **<ymax>** NE Y corner of the considered high resolution area,
- **<r_area>** set high resolution area.

Setting up the boundary conditions on the simulation domain:

- **<boundN>** Northern boundary condition,
- **<boundS>** Southern boundary condition,
- **<boundE>** Eastern boundary condition,
- **<boundW>** Western boundary condition.

Possible values for these fields are 0,1,2**.** Where 0 defines a fixed boundary, 1 a wall and 2 a slope boundary. By default the value is set to 2 for all borders.

- **<outlet>** defines an outlet on one of the corner of simulation area (allowed values are: 1 for SW corner, 2 for SE corner, 3 for NW corner and 4 for NE corner). When defining an outlet the previous boundary conditions will be set to 1 (wall boundary).

Time

<struct_time>

The second structure defines simulation and processes time steps.

- **<time_start>** starting time of the simulation,
- **<time_end>** ending time of the simulation,
- **<display_interval>** time interval to create output.

In addition and if we are restarting a previous simulation:

- **<restart_folder>** name of the previous simulation folder,
- **<restart_fileID>** time interval of the restarted simulation,
- **<restart_petNb>** number of processors used in previous run,
- **<time_step>** set minimum time step for the run.

Forcing parameters

Sea-level fluctuations

<struct_ocean>

Optional structure which define ocean fluctuations.

<ocean_file>name of the file containing the sea level evolution through time. This **ASCII** file provides for each line the following information:

- time in years,
- sea-level elevation for the considered time in meters.

In addition the defined fluctuation times should be set in increasing order starting from the oldest time.

Uplift/subsidence evolution

<struct_geodyn>

Optional structure which define tectonic displacements.

- **<fields_3D>** should be set to 1 if horizontal displacements are used (default value is set to 0),
- **<merge_dist>** the minimal distance (in meters) between two TIN nodes under which point merging algorithm is performed (required if **<fields_3D>** is equal to 1),
- **<interval_nb>** total number of displacement intervals that will be simulated. The displacement intervals need to be declared by increasing time and should not overlap with each others,
- **<disp>** definition of an individual displacement field,
- **<disp_start>** time in years at which the considered vertical displacement will start,
- **<disp_end>** Time in years at which the considered vertical displacement will end,
- **<disp_file>** name of the displacement file and its associated path. The path is from the main input file location.

The displacement **ASCII** file provides at each line the cumulative vertical displacement for each considered node in meters.

Attention: the file defines the cumulative displacement during the duration defined above and not a displacement rate.

Note: the nodes are read in increasing order based on the regular grid discretization starting from the South-West corner and going first along the X axis (West to East).

Climate evolution

<struct_rainfall>

To simulate overland flows it is essential to defines rainfall parameters. It is possible to specify a series of maps with rainfall values defined for each nodes.

<rain_nb> defines the number of rainfall series imported for the considered simulation.

<rain> collection of rainfall parameters defining each series.

Note: the number of classes needs to be equal to the number given in the **<rain_nb>** element.

- **<rain_start>** start time of the considered rainfall grid interval in years,
- **<rain_end>** end time of the considered rainfall grid interval in years,
- **<rain_file>** name of the rainfall file and its associated path. The path is from the main input file location.

OR

- **<rain_value>** in case the rainfall is uniform over the simulation it is possible instead of using an external **ASCII** file **<rain_file>** to define the value within the XmL file directly (in meters/year).

This **ASCII** file provides for at each line the averaged precipitation in meters/year.

Note: the nodes need to be defined in increasing order based on the regular grid discretization starting from the South-West corner and going first along the X axis (West to East)

Note: in case a specific node does not have any precipitation it is required to set it in the file with a 0.0 value.

Overland flow parameters

Detachment limited

<struct_detachment>

Model equation:

$$\mathbf{q_r} = -\kappa_r (q_w)^m (\nabla z)^n$$

For detachment limited transport (stream power law), the following parameters are required.

<spl_m> corresponds to the coefficient m in the equation.

<spl_n> corresponds to the coefficient n in the equation.

<Cerodibility> corresponds to the coefficient κ_r in the equation.

In case where you are interested in purely erosive system the optional element below could be set to increase the computational time:

<pureErosion> to take into account erosion only, possible values are 0 or 1.

Hillslope parameters

Simple creep

<struct_linear_diff>

Model equation:

$$\mathbf{q_d} = -\kappa_d \nabla z$$

For simple creep, the following parameters are required:

<coef_linear_aerial> κ_d parameter in aerial environment.

<coef_linear_marine> κ_d parameter in marine environment.

Sediment loading

Flexural isostasy & compaction

<struct_flex>

<flex_dt> flexural isostasy & compaction computation time step (a multiple of the display interval time),

<flex_dx> spatial discretization of the flexural grid in meters (values are around several kilometers),

<sed_dens> sediment density (kg/m^3),

<mantle_dens> mantle density (kg/m^3),

<flex_thick> elastic thickness (in meters),

<flex_order> choice is 2 (13-point second-order grid approximation) or 4 (four-order multi-grid solutions to the biharmonic equation),

<nb_Pfields> number of lithostatic pressure in the porosity table.choice is 2 (13-point second-order grid approximation) or 4 (four-order multi-grid solutions to the biharmonic equation),

<pressure_val> lithostatic pressures values (in GPa),

<porosity_val> associated porosity values for considered lithostatic pressures.

Visualization

Output

<output_directory>

Name of the output folder where both simulation results and run files will be stored. The directory is divided in two sub-directories:

- one called **outputs** which record simulation output,
- one called **runfiles** which record simulation informations

Note: the outputs sub-directory contains time-series files that can be visualized in **Paraview** or **Visit**.

Note: the **runfiles** sub-directory contains the checkpointing files required to restart a simulation.

Note: to preserve previous runs, you will have to change the output directory name otherwise it will be automatically rewritten and previous outputs will be lost.

CHAPTER 3

Badlands model: examples

All tests provided in the following section are available from GitHub
Badlands-doc v1.0

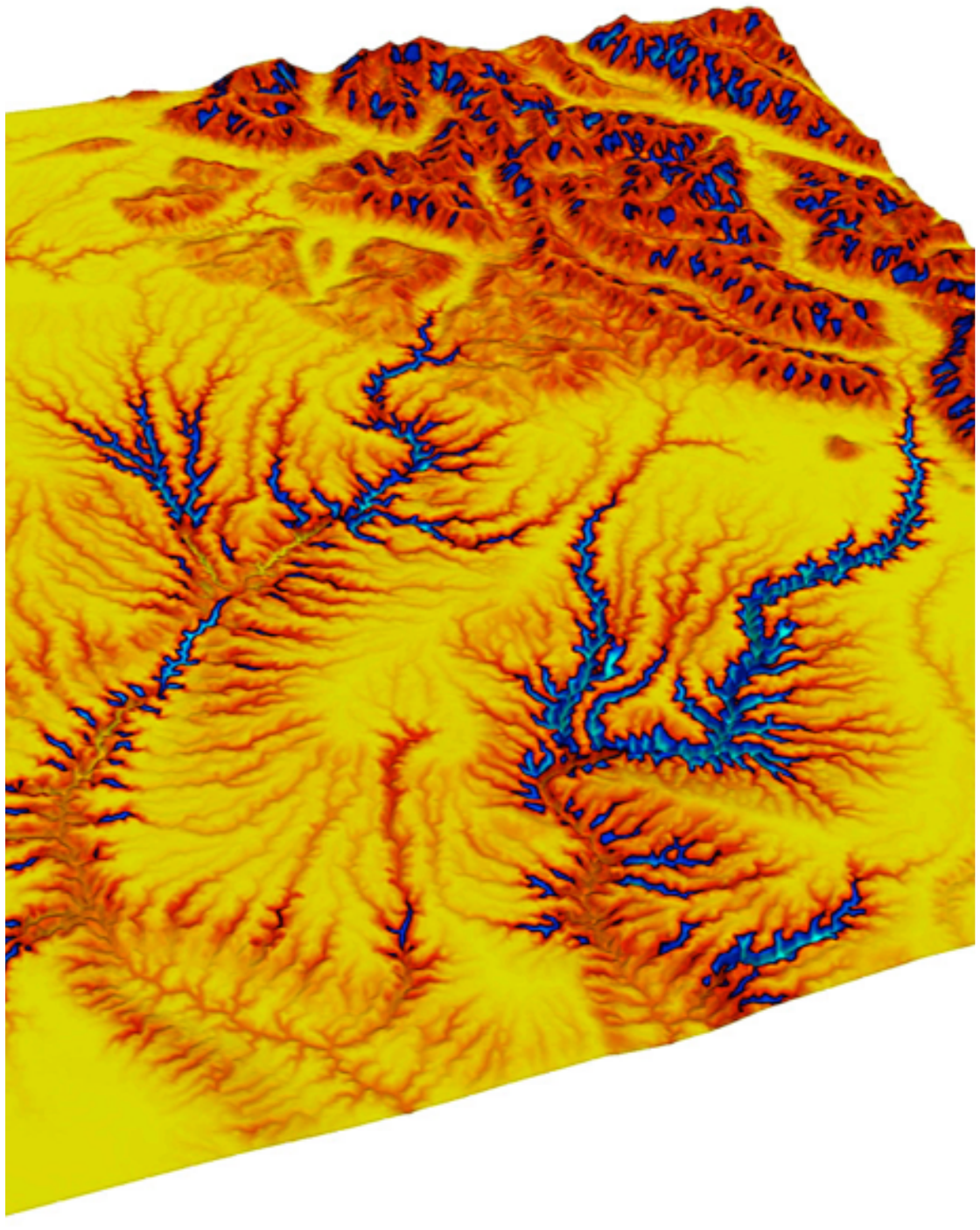

Rise of the Phoenix! Badlands simulation.

Section 1

Planar surface with single outlet

Key Points

1. Experimental settings.
2. River profile.
3. Sensitivity analysis.

Planar surface with single outlet

Initial conditions

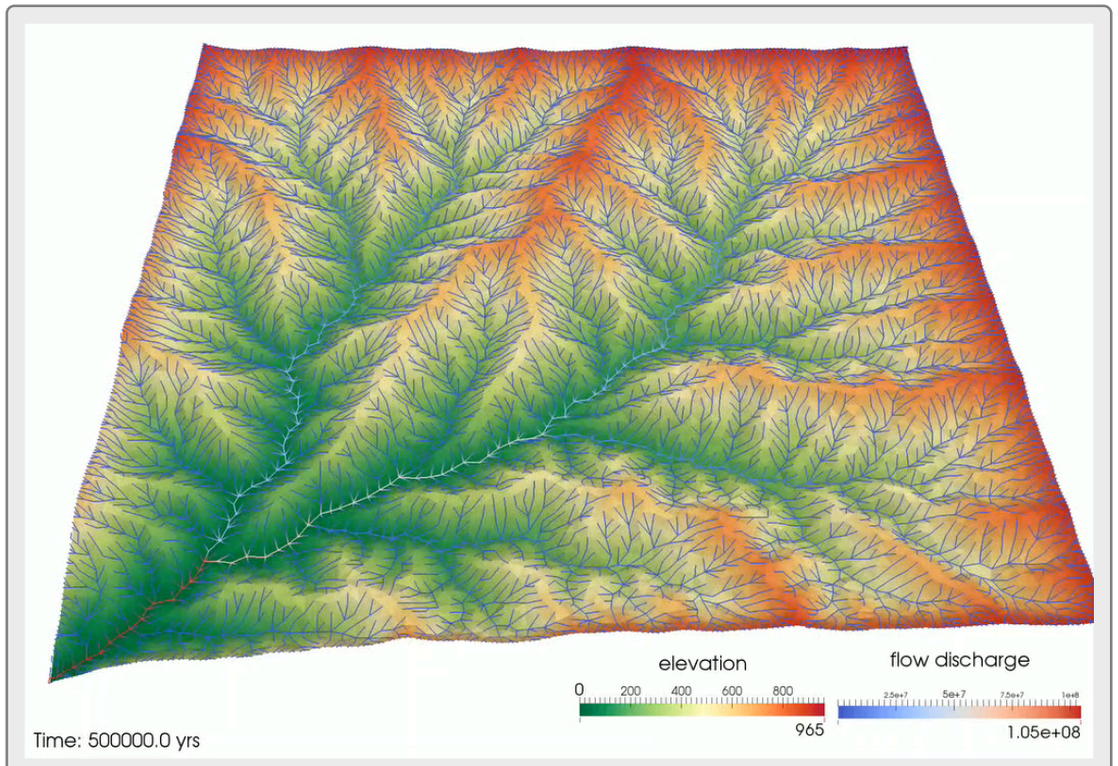

Surface evolution of a horizontal plane with a single outlet subject to uniform uplift and rainfall.

Above animation shows an example of surface simulation starting from a horizontal topographic surface of size 10×10 km^2, sampled randomly on about 10,000 points, that evolves through a time span of 500 kyr. The uplift rate is set to 1 mm/yr everywhere except on the outlet point where a subsidence of 0.2 mm/yr is imposed. The rainfall is set to 1 m/yr over the entire domain. All surface boundary points are closed, except for a single open outlet at $(0,0)$ coordinates. This surface is allowed to evolve by simulating linear diffusion (*simple creep*) and detachment limited overland flow processes. Diffusion is implemented with a uniform diffusivity constant $\kappa_d = 0.1\ m^2/yr$. Erosion due to channeling is simulated with the following parameters: $\kappa_r = 10^{-5}\ m^{1-2m}/yr$; $m = 0.5$;

$n = 1$. Note that, in this simulation, all the model parameters are constant and uniform. The only spatially random element is given here by the position of the sampled points. A developed drainage network is already visible after 50 kyr evolution, as a result of competition between diffusive hillslope transport and channel incision processes. After 250 kyr, the surface has evolved and forms a fully developed, dendritic drainage pattern with maximum stream order of 7 over the last portion of the catchment just before reaching the outlet. Over the last 200 kyr the drainage pattern is stabilized.

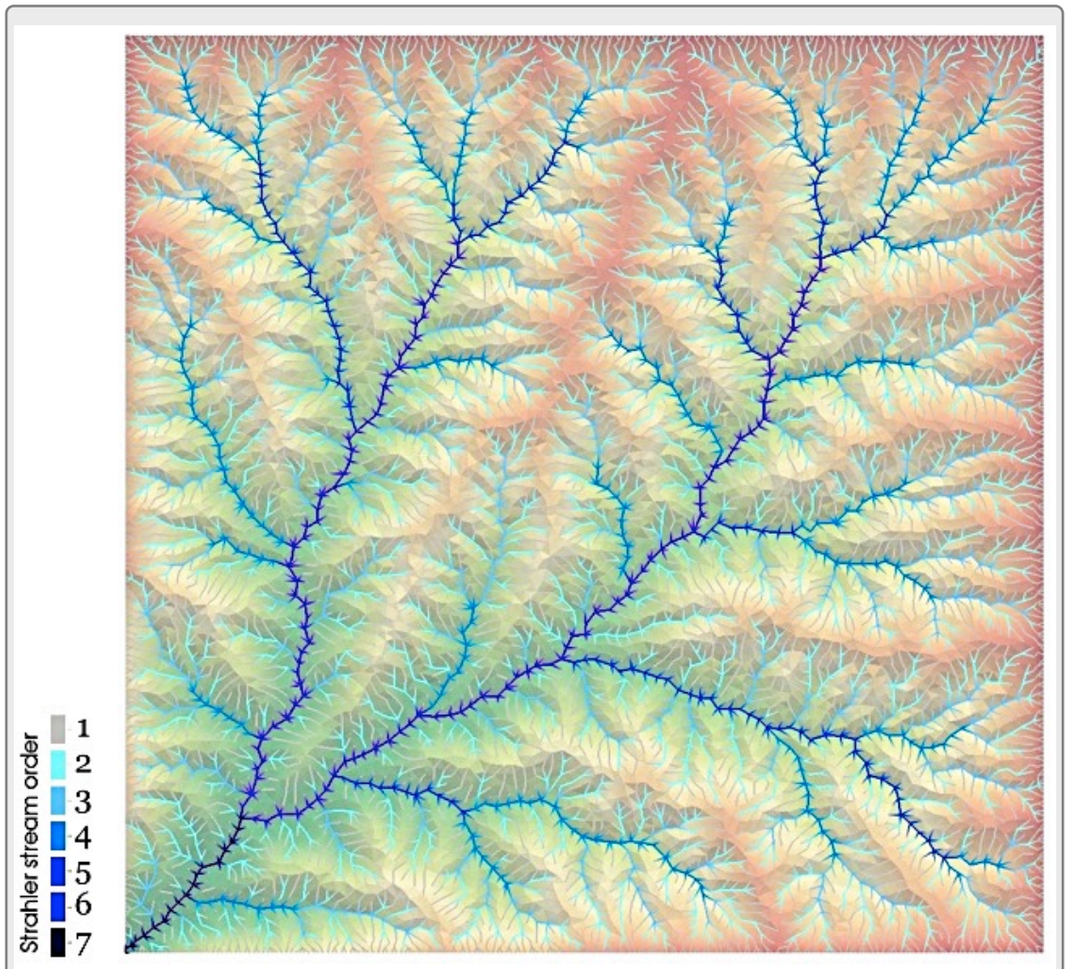

Strahler stream order after 500 kyr

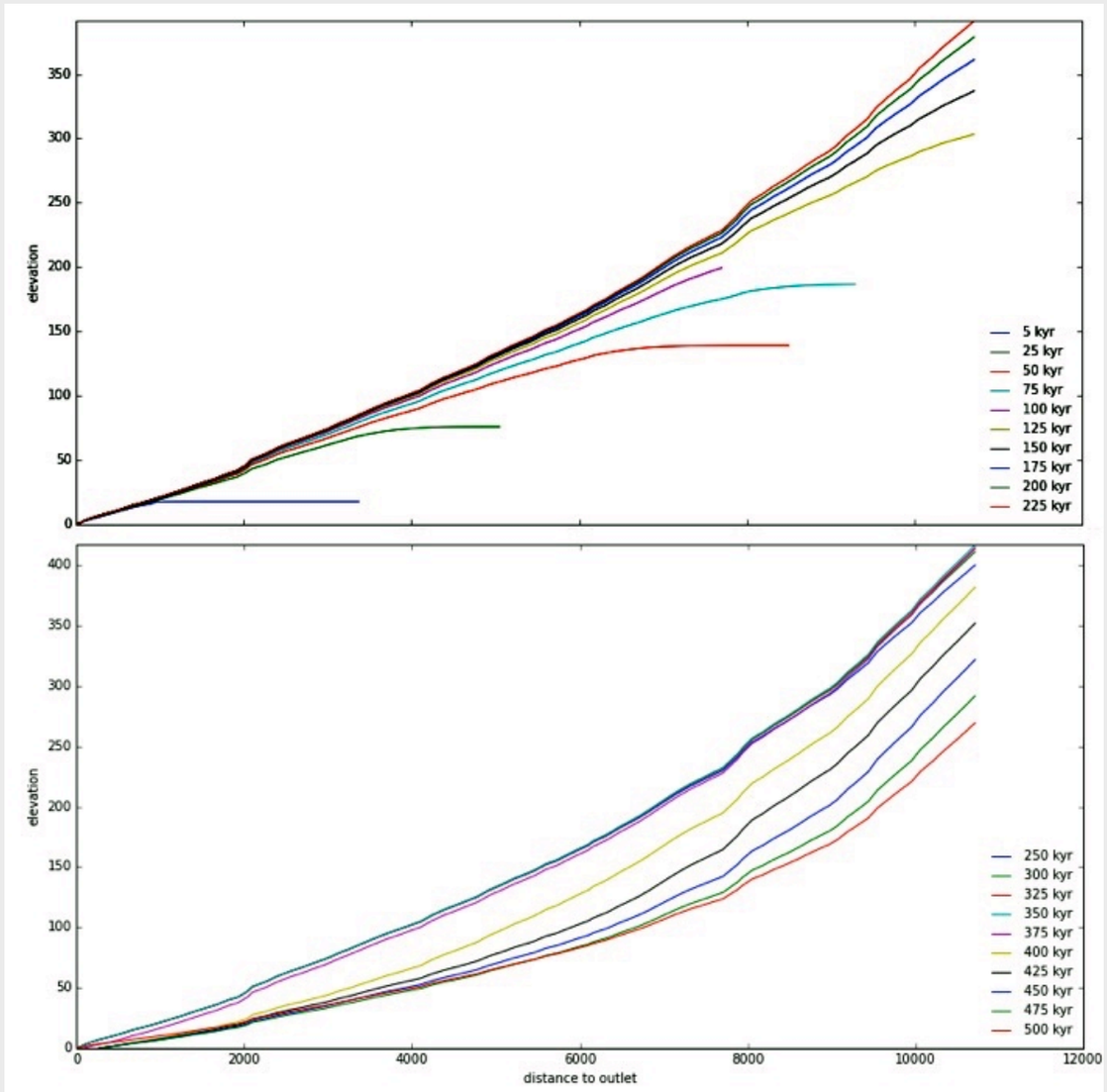

Evolution of the river profile. Top: propagation of the erosion front during the first 250 kyr. Bottom: construction of a concave profile.

River profile evolution

To underline more quantitatively the consistency of the simulation, it is possible to represent a series of profiles of one particular river (the longest visible blue line roughly on the bottom diagonal of the squared domain) extracted from the TIN surface. We observe the progression of of erosion in the upslope direction as time passes (top figure), indicated

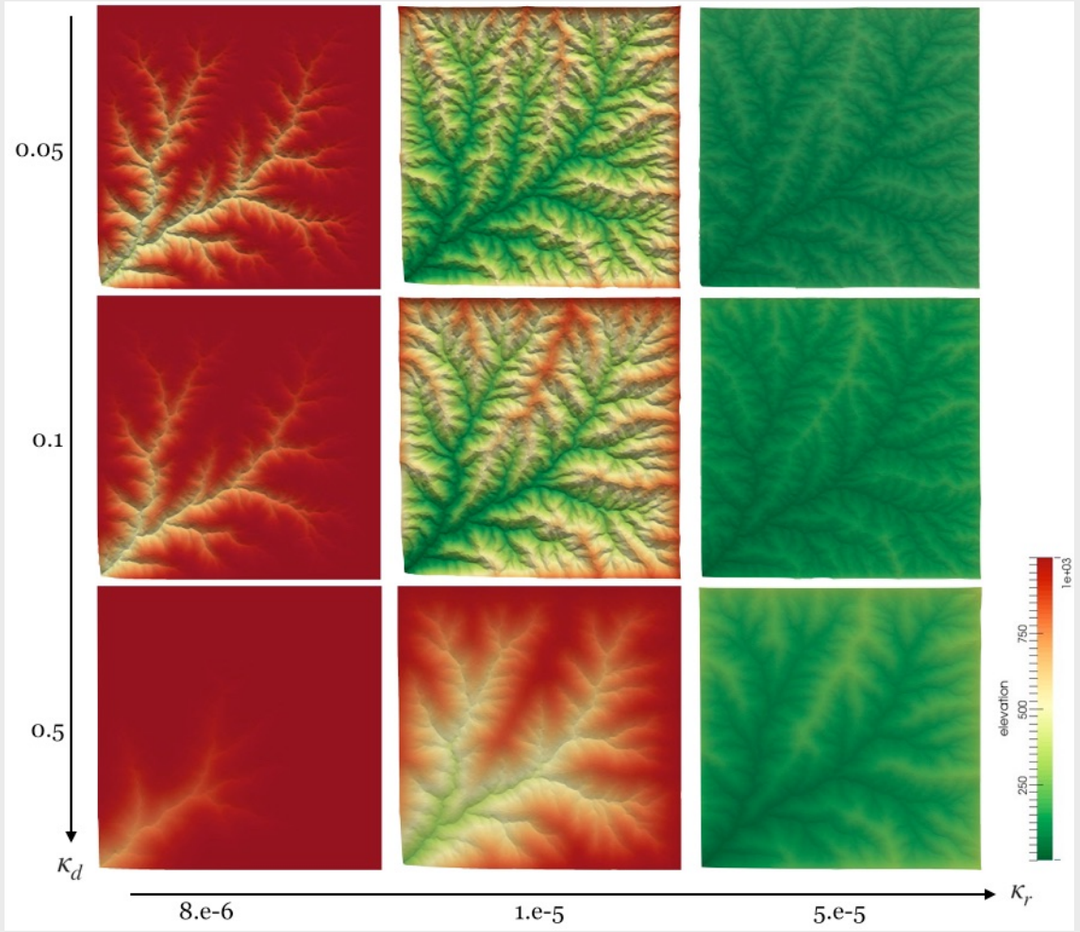

Sensitivity analysis of landscape evolution for different diffusion κ_d and the detachment-limited κ_r coefficients. The results are shown after 500 kyr.

symbolically by the grey arrow. By a simulated time of 200 kyr, the entire river course has settled and the river profile shows an upward concavity (bottom figure).

Sensitivity Analysis

Model sensitivity to both diffusion and detachment limited coefficient is explored for 3 different values of κ_d and κ_r. The results presented in the next figure shows how the landscape has evolved for a considered period of 500 kyr. We observe that increase in hillslope processes magnitude (increase in κ_d) leads to a "*smoothing*" of surface topography but does not produce changes in the final morphology of the river network. The effect of κ_r is tested by varying it between $8.10^{-6} - 5.10^{-5}$. Because it is a constant of proportionality, varying κ_r influences the rate of landscape evolution; if κ_r is increased by more than 10 for the considered set of model parameter, the landscape erodes nearly instantaneously.

References

Refice, A. Giachetta, E., Capolongo, D. (2012). SIGNUM: a Matlab, TIN-based landscape evolution model, Computers & Geosciences 45, 293-303.

Castelltort, S. Yamato, P. (2013). The influence of surface slope on the shape of river basins: Comparison between nature and numerical landscape simulations, Geomorphology 192, 71–79.

SECTION 2

Delta evolution & sea-level fluctuations

KEY POINTS

1. Experimental settings.
2. Hillslope & overland flow models.
3. Depositional/erosional patterns.
4. Stratigraphic evolution.

SEDIMENT TRANSFER, DELTA FORMATION AND SEA-LEVEL VARIATION

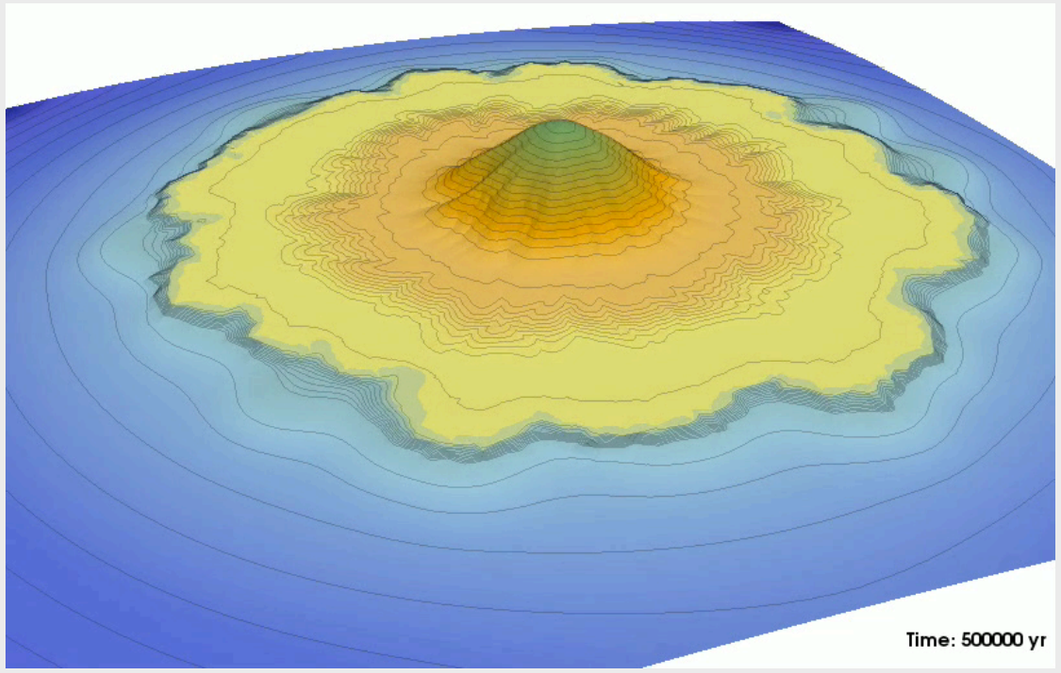

Mountainous landscape evolution with sedimentation front evolving over time subject to sea-level fluctuations.

EXPERIMENTAL SETTINGS

The initial surface defines a mount which is a half ellipsoid of 2000 m height and about 8 km large (youtube video). The sea-level is initially set at the base of this mount at a elevation of 0 m. An uniform precipitation rate of 1 m/yr is applied on the all area and we test the evolution of the surface due to both hillslopes and overland flows. Two hillslope coefficient are defined for both the aerial and marine area. The simulation runs for $500{,}000$ years and we vary the sea-level through time (values are defined in table next page). From its initial setting, we first perform a sea-level drop of 100 m after $200{,}000$ years than we come back to the initial sea level at $300{,}000$ years. We then perform a second cycle, this time by imposing a sea-level rise of 100 m for around $100{,}000$ years,

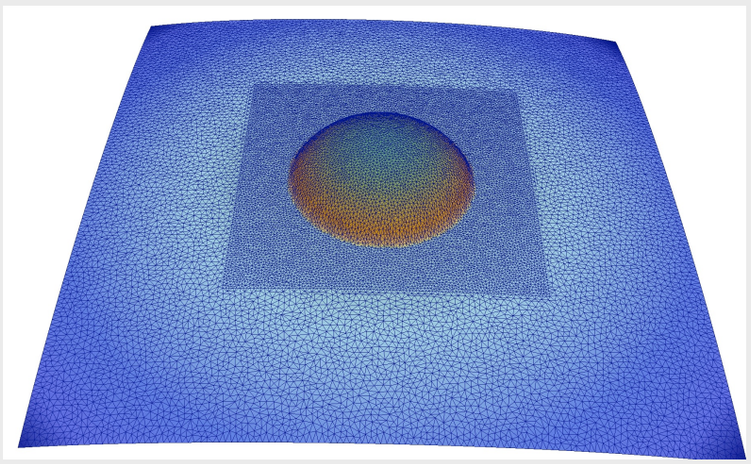

Initial setting showing the 2 resolutions generated by Badlands.

TIME	SEA LEVEL
0	0
180,000	0
200,000	–100
280,000	–100
300,000	0
320,000	100
380,000	100
400,000	0
500,000	0

then finally, we reset the sea-level to 0 m until the end of the simulation.

In addition, the grid is divided in two resolutions by defining a bounding box within the input file. A high-resolution area ($10{,}000\ m^2$) is chosen around the mount, whereas the marine environment has a lower resolution of $40{,}000\ m^2$.

Depositional/erosional patterns

During the first phase of the simulation the mount is eroded and sediment are transported in the marine environment where we see a sedimentation front prograding towards the marine environment (two top views in the next figure).

As the sea-level falls, it creates a condition of forced regression, in which the coast is forced to build seaward. During the falling stage, rivers begin to incise on what was formerly a marine shelf, forming incised valleys. These incised valleys tend to widen and grow landwards. From $200{,}000 - 280{,}000$ years, the low-stand system marks the greatest extent of subaerial exposure and erosion.

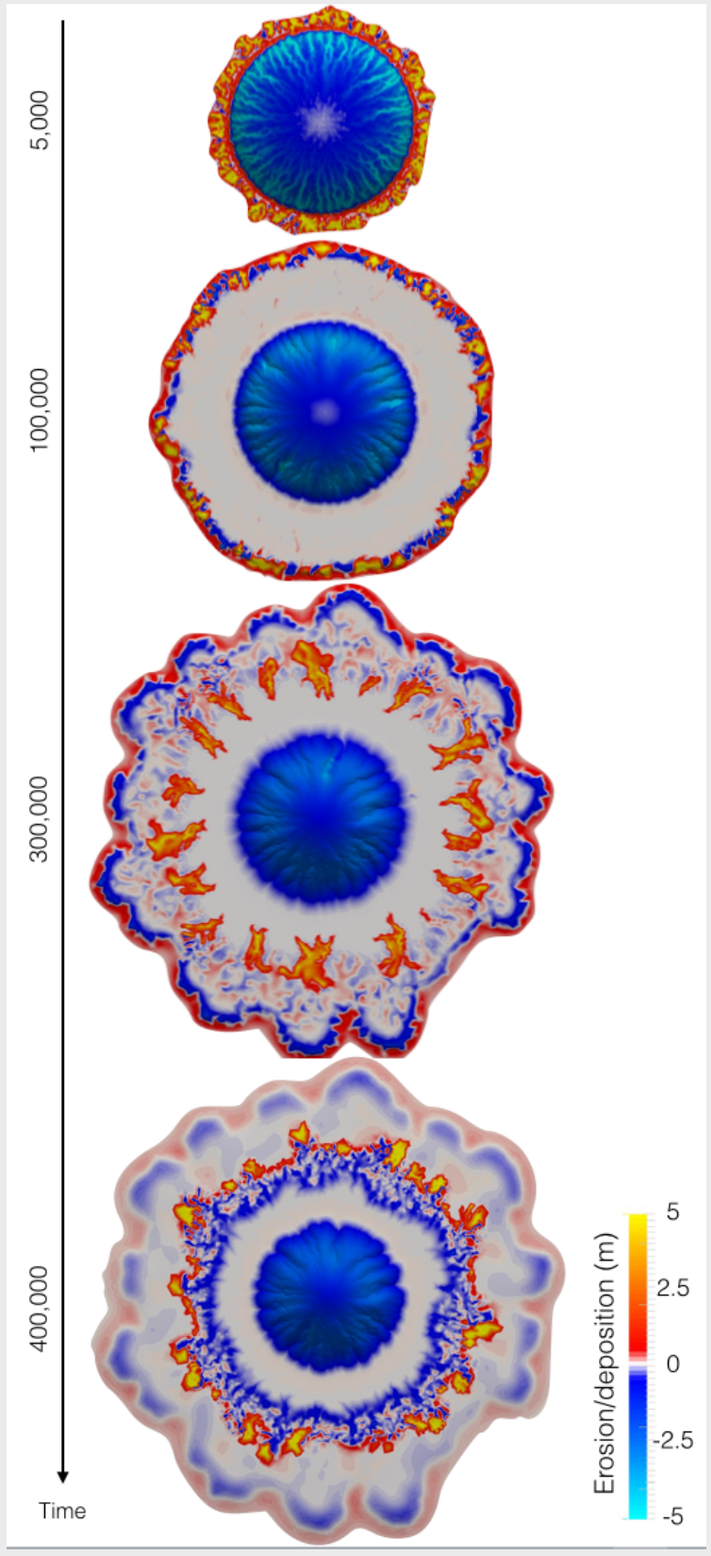

Evolution through time of the mountain due to uniform rainfall and sea-level fluctuations, showing area of erosion and deposition.

As the rate of relative sea-level rise increases, it leads to retrogradational parasequence stacking also refers as transgressive systems. During this stage the the previously incised valleys are filled as shown in the previous figure at $300{,}000$ years.

Between $320{,}000 - 380{,}000$ yrs, the sedimentary system turns from retrogradational stacking in the transgressive system to progradational stacking in the highstand system. During this stage, the sediment supply to the shelve favors the development of progradational sequences.

During the last $100{,}000$ years, the system returns to its original sea-level which is mark by incision of formerly marine shelf deposits and development of a new sedimentation front.

References

Coe, A. L., 2002. The Sedimentary Record of Sea-Level Change. Cambridge, New York: Cambridge University Press. pp. 57–98

Hampson, G.J., Davies, S. J., Elliott, T., Flint, S. S., Stollhofen, H., 1999. Incised valley fill sandstone bodies in Upper Carboniferous fluvio-deltaic strata: recognition and reservoir characterisation of Southern North Sea analogues. In: Petroleum Geology of NW Europe: Proceedings of the 5th Conference. (Edited by Fleet, A.J. & Boldy, S.A.R.). The Geological Society, London. 771-788.

SECTION 3

Climatic forcing on drainage evolution

KEY POINTS

1. Experimental settings.
2. Natural analogues.
3. Temporal evolution of catchments.

ROLE OF CLIMATE CHANGE IN DRAINAGE NETWORK REORGANIZATION

The continuous feedbacks among tectonics, surface processes, and climate change are reflected in the distribution of catchments on active mountain fronts.
Previous studies have shown a certain regularity of valley spacing on several mountain ranges worldwide, but what is at the origin of such geomorphological feature of landscapes is currently not well known.

This example illustrate long-term landscape evolution of an active mountain range. It shows how the constant valley spacing, achieved at steady state on both sides of the range, is progressively restored after simulating a migration of the main drainage divide caused by a precipitation gradient applied across the mountain belt.

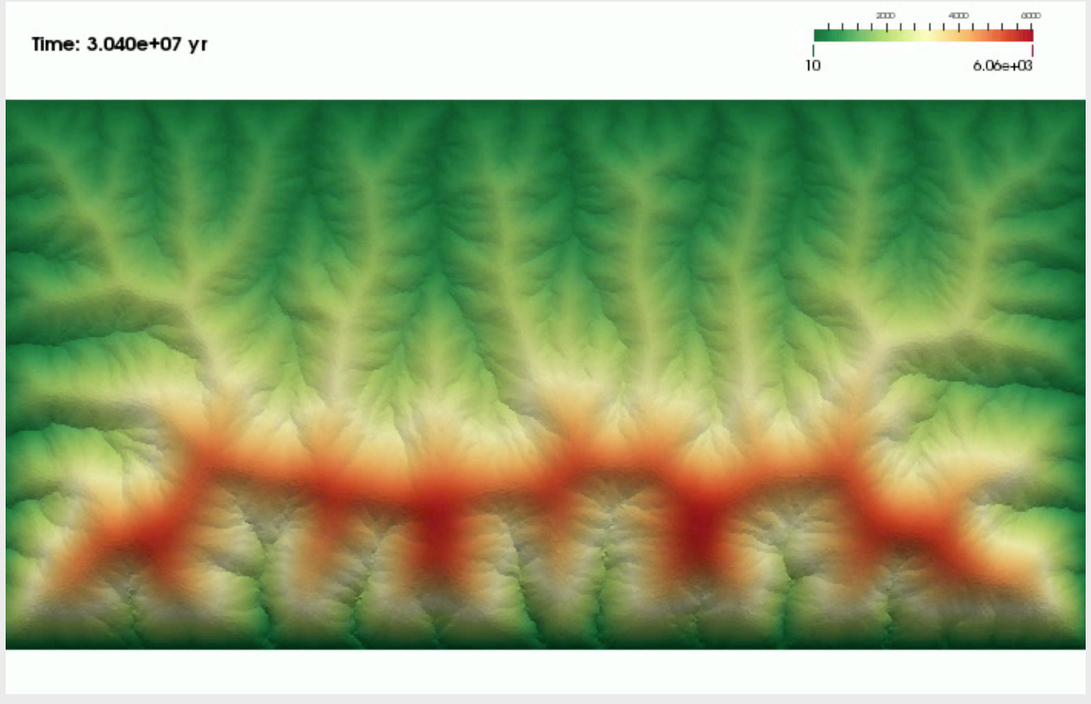

From an initial steady state, drainage network reorganization under an imposed precipitation gradient.

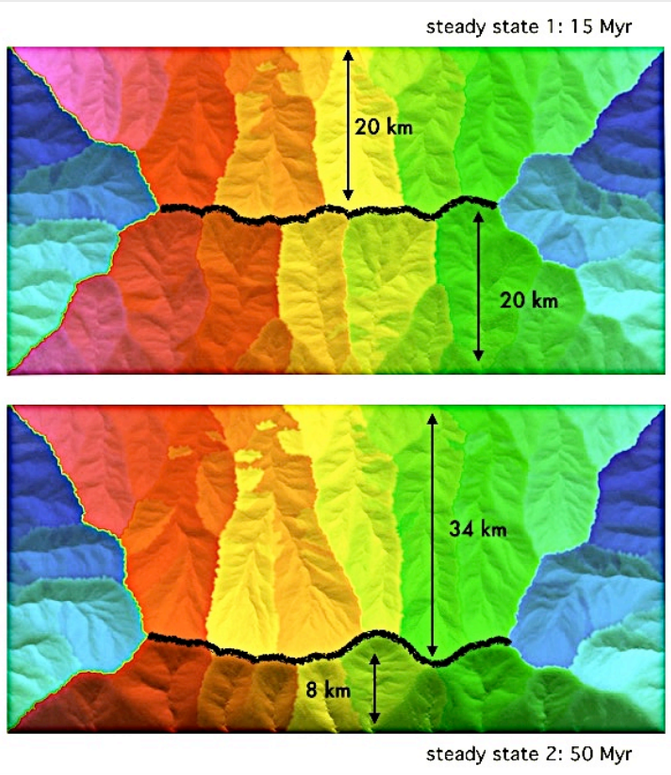

Top: landscape has reached the steady-state topography under uniform precipitation. Bottom: development of the second steady-state topography under a precipitation gradient. Middle line shows the drainage divide for both states.

Experimental settings

We simulate landscapes of various sizes, with a fixed TIN mean sampling distance of 100 m; the initial surface is completely flat at zero elevation. Sediment can flow across all four landscape boundaries. We apply a spatially uniform and constant uplift rate of 1 mm/yr over the whole domain.

After the initial topography has reached a steady state under a uniform, constant precipitation rate of 1 m/yr, a precipitation gradient is introduced, in a direction perpendicular to the belt axis, to simulate "orographic" precipitation; the maximum precipitation rate is set to 3 m/yr along the upper side, and it linearly decreases towards the opposite side reaching a minimum of 0.1 m/yr.

Temporal evolution of river catchments

The landscape reached the first steady-state topography under uniform precipitation after 15 Myr. The pattern of catchments, illustrated in the top right figure, consists of an alternation of larger, and smaller catchments etched on the triangular facets. The catchments on the North and South side of the mean drainage divide exhibit the same elongated characteristics.

Drainage network evolution for a considered catchment after imposing the precipitation gradient.

After the precipitation gradient is applied, the main divide of the belt is pushed from the wet side (northern part) towards the dry side (southern part), where larger catchments shrink and, simultaneously, the smaller catchments on triangular facets grow. Furthermore, the drainage network and maximum stream order is consequently reduced in the larger watersheds.

A new steady state topography is reached under changed climatic conditions. The numerical results show that change in the precipitation pattern exerts a strong control on drainage network development and reorganization on both sides of the simulated mountain belt. In particular, the leeward side shows a more interesting evolution, where the interaction amongst all geomorphic processes leads to a significant catchment reorganization.

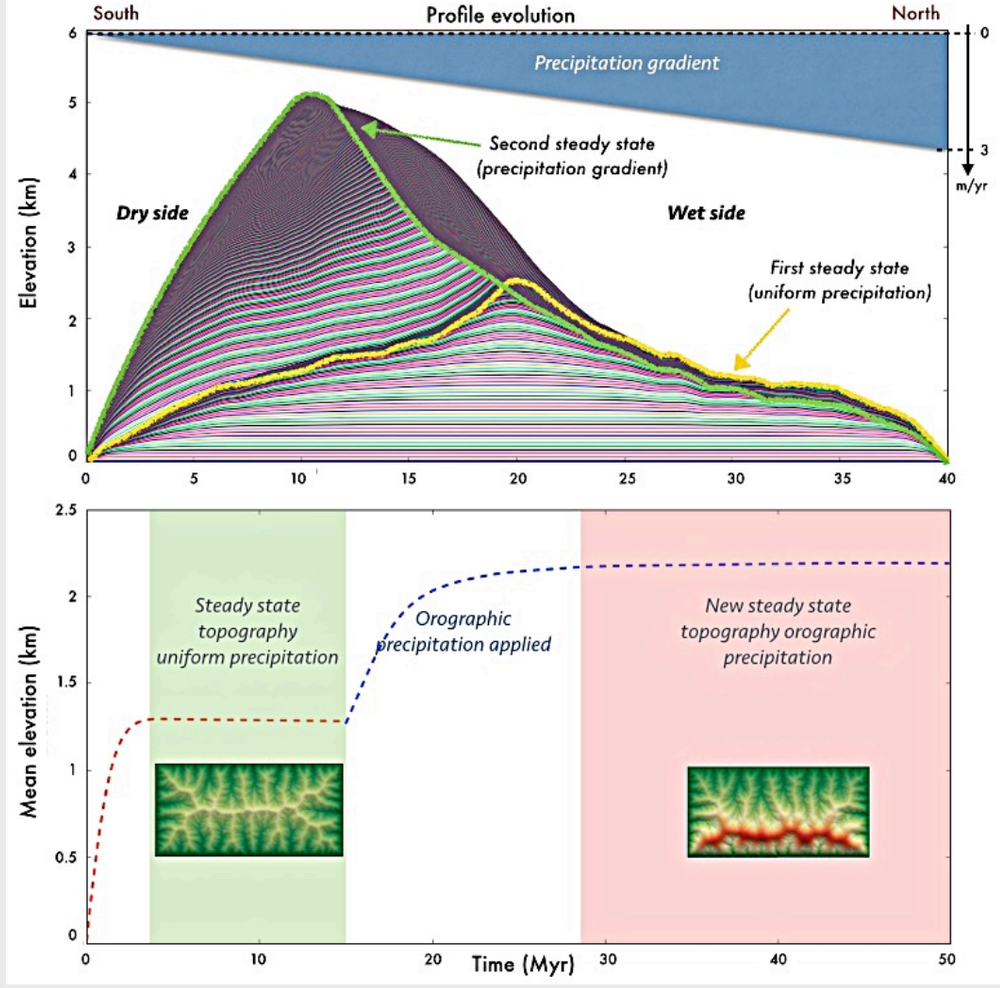

Top: average evolution of landscape profile across the mountain range illustrating the migration of the mean drainage divide towards the dry side when the orographic precipitation is applied. Bottom: plot of the mean landscape elevation over time representing the two steady states topography.

The final result of this complex mechanism of watershed reorganization is a new steady state topography.

Furthermore, the model of watersheds development proposed here, can explain some real landscapes in which we found analogies with the different evolutionary stages of the simulated belts.

REFERENCES

Bonnet, S. (2009). Shrinking and splitting of drainage basins in orogenic landscapes from the migration of the main drainage divide, Nature Geoscience, 2:11, p. 766-771.

Daly, C., Neilson, R.P., and Phillips, D.L. (1994). A statistical-topographic model for mapping climatological precipitation over mountainous terrain. Journal of Applied Meteorology, v. 33, 140–158.

Ellis, M., Densmore, A.L., and Anderson, R.S. (1999). Development of mountainous topography in the Basin Ranges, USA, Basin Research, v. 11, p. 21–41.

Hovius, N. (1996), Regular spacing of drainage outlets from linear mountain belts, Basin Research, 8, 29-44. Perron, J.T., Kirchner, J.W., and Dietrich, W.E. (2009). Formation of evenly spaced ridges and valleys, Nature 460, 502-505.

PRISM Climate Group (2006), Oregon State University: http://prism.oregonstate.edu.

Refice, A. Giachetta, E., Capolongo, D. (2012). SIGNUM: a Matlab, TIN-based landscape evolution model, Computers & Geosciences. 45, p. 293-303.

Tucker, G.E., Lancaster, S.T., Gasparini, N.M., Bras, R.L. and Rybarczyk, S.M. (2001). An Object-oriented Framework for Distributed Hydrologic and Geomorphic Modeling using Triangulated Irregular Networks. Computers & Geosciences. 27: 959-973.

Wallace, R.E. (1978). Geometry and rate of changes of fault-generated range fronts, northcentral Nevada. Jour. Research U.S. Geol. Survey, 6, 637-650.

SECTION 4

High-resolution depression filling model

KEY POINTS

1. Experimental settings.
2. Pit evolution.
3. Crater filling.

PIT CRATER GEOMORPHOLOGICAL EVOLUTION

Central pit craters are a crater type that contain an approximately circular depressions in their floor or central peak. These craters have been found on Earth, Mars, Ganymede, and Callisto. Here we use their typical shape to perform a high resolution simulation using Badlands depression filling method.

EXPERIMENTAL SETTINGS

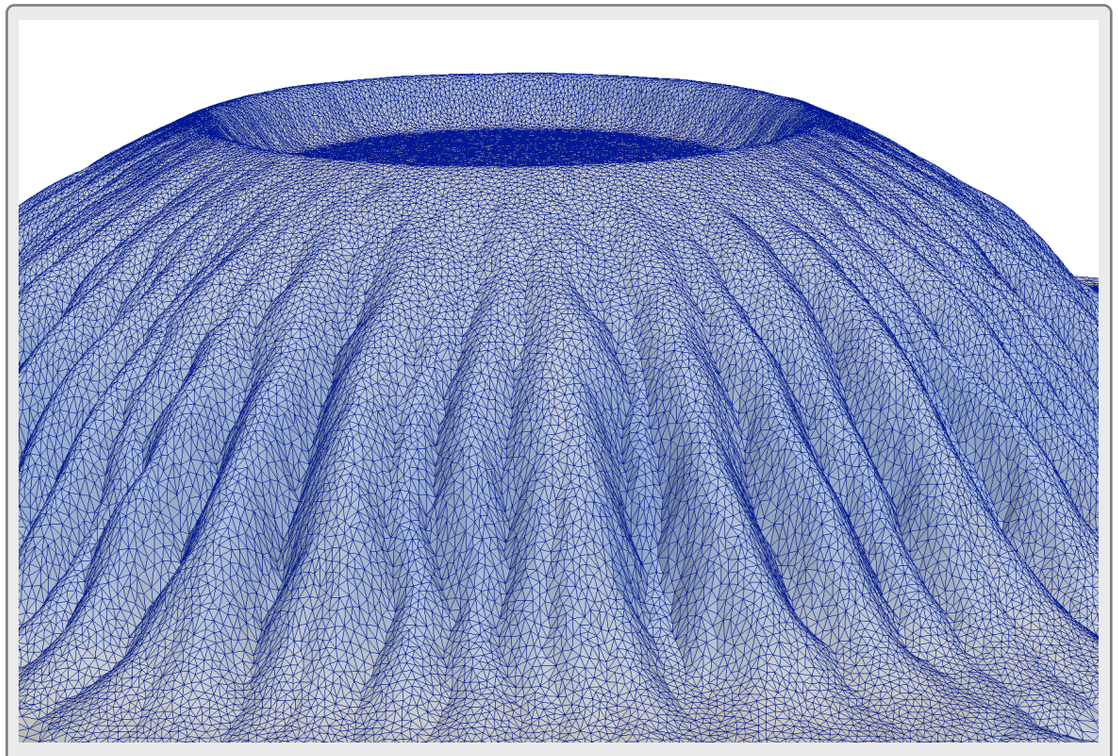

Illustrating of TIN node connectivity of the edge of the pit crater.

In this example, we impose over $100{,}000$ years a constant precipitation rate of 1 m/yr over an initial 2×2 km crater if 250 m depth. The resolution of the TIN is lower than 10 m.

PIT EVOLUTION

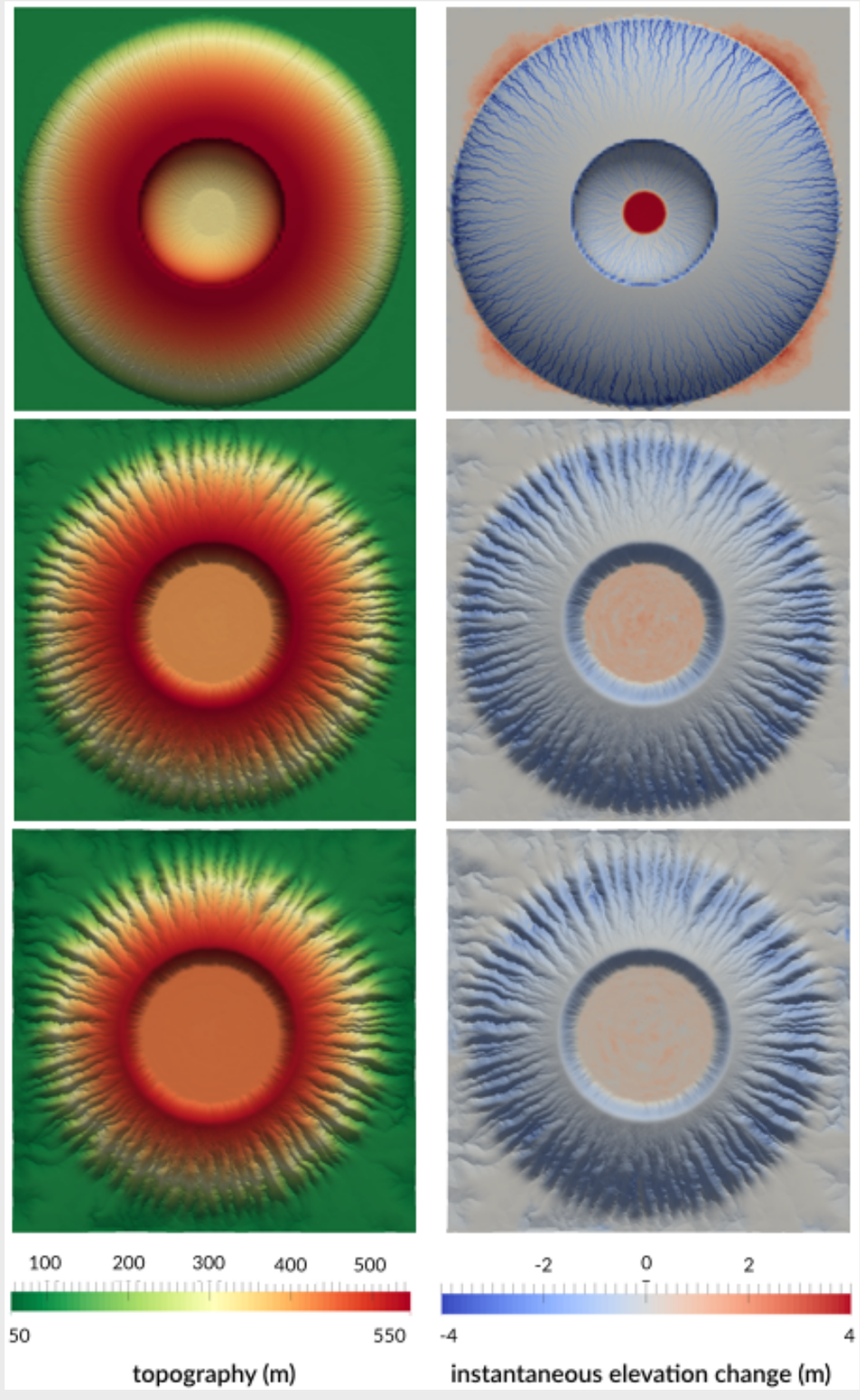

Progressive filling of the pit crater through time (top 1,000 years, middle 50,000 years and bottom 100,000 years).

Simulated fluvial stream power law implies the infill of the crater bottom with alluvial fan deposits, whereas the crater rim gradually backwastes while maintaining a generally steep slope.

Both the backwasting and the downcutting of the crater rim occur, so that in later stages of erosion the crater may become essentially rimless.

Crater infilling

Degradation of craters by fluvial erosion and deposition in this simulation results in rapid initial infilling but a slowing rate through time likely due to the decreasing height of interior crater walls and the increasing area of deposition as the crater enlarges due to crater wall erosion. The result is in agreement with several other studies on this specific type of morphology (Forsberg-Taylor et al, 2004; Howard, 2007).

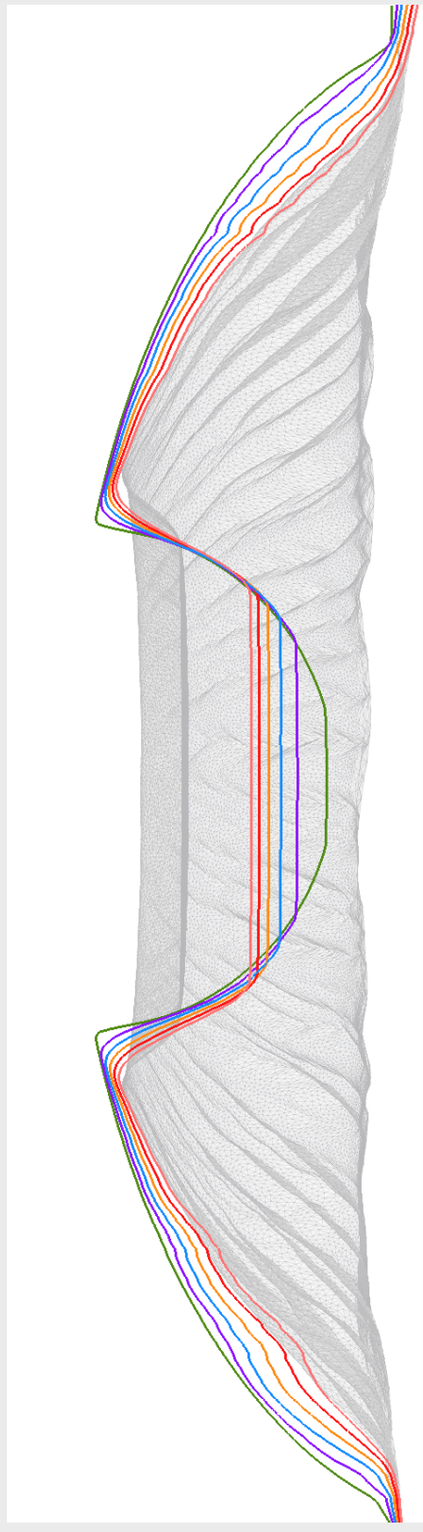

Section view of the continuous erosion of the external side of the pit crater and filling of the internal depression.

REFERENCES

Forsberg-Taylor, N.K., Howard, A.D. and Craddock, R.A., 2004. Crater degradation in the Martian highlands: Morphometric analysis in the Sinus Sabaeus region and simulation modeling suggest fluvial processes. Journal of Geophysical Research, 109: doi:10.1029/2004JE002242.

Howard, A. D. (2007), Simulating the development of Martian highland landscapes through the interaction of impact cratering, fluvial erosion, and variable hydrologic forcing, Geomorphology, 91, 332–363, doi:10.1016/j.geomorph.2007.04.017.

Section 5

3D tectonic coupling and drainage evolution

Key Points

1. Pull-apart basins.
2. Displacement fields parameters.
3. Basins evolution.

Pull-apart basins

Interlinks between deformation and sedimentation have long been recognized as an important factor in the evolution of continental rifts and basins development. However, determining the relative impact of tectonic and climatic forcing on the dynamics of these systems remains a major challenge.

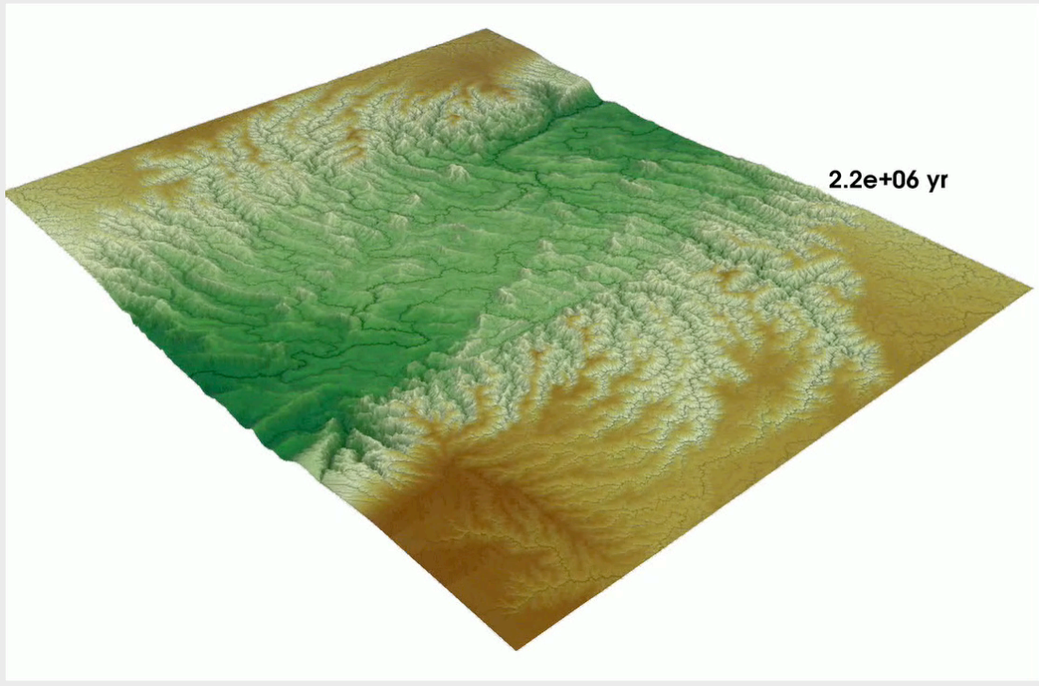

2.2 millions years of landscape evolution in a pull-apart setting.

Experimental settings

In this example, we impose over $2{,}000{,}000$ years a $3D$ displacement field produced with *Underworld* over an initial flat surface. We consider both hillslope (creep) and overland flow processes (detachment limited) induced by an uniform precipitation rate of 1 m/yr.

The 3D displacement field obtained from *Underworld* gives us an average rate which is updated every $5{,}000$ years. The model is initially a 256 km square box at a resolution of 1 km. The video for this model is avail-

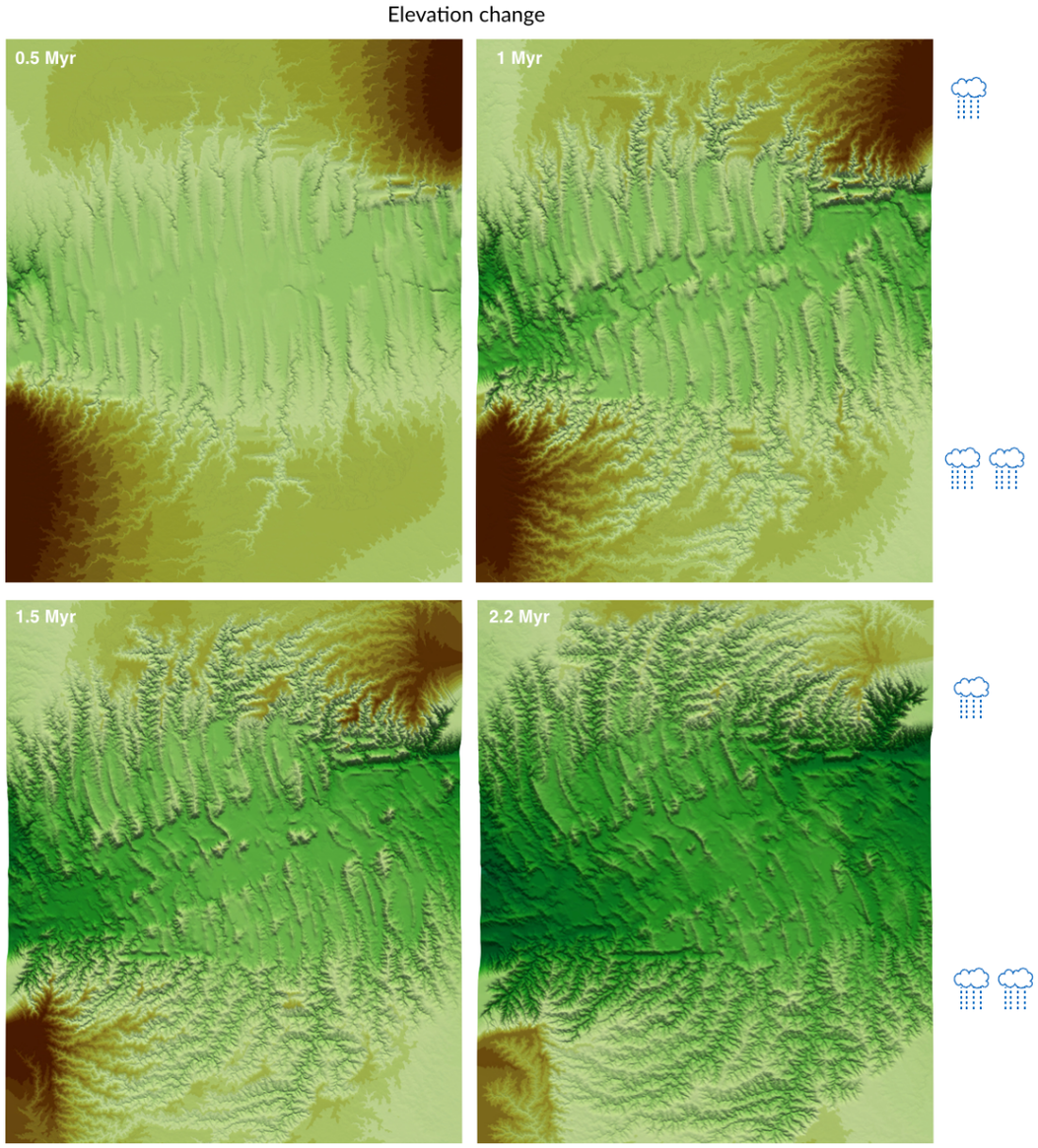

Drainage network evolution due to 3D deformations and a precipitation gradient (dry side on the northern part and wet on the southern area)

able on here. We test with **Badlands** the effects of high horizontal displacement rates on landscape geomorphological evolution. It is important to note that just the first displacement files for running the first thousands years are provided here.

Displacement fields

Pull-apart basins are depressions that are bounded by sideways-stepping, strike-slip faults parallel to their length. They form where the sense of stepping or bends along the faults have the same sense as fault motion.

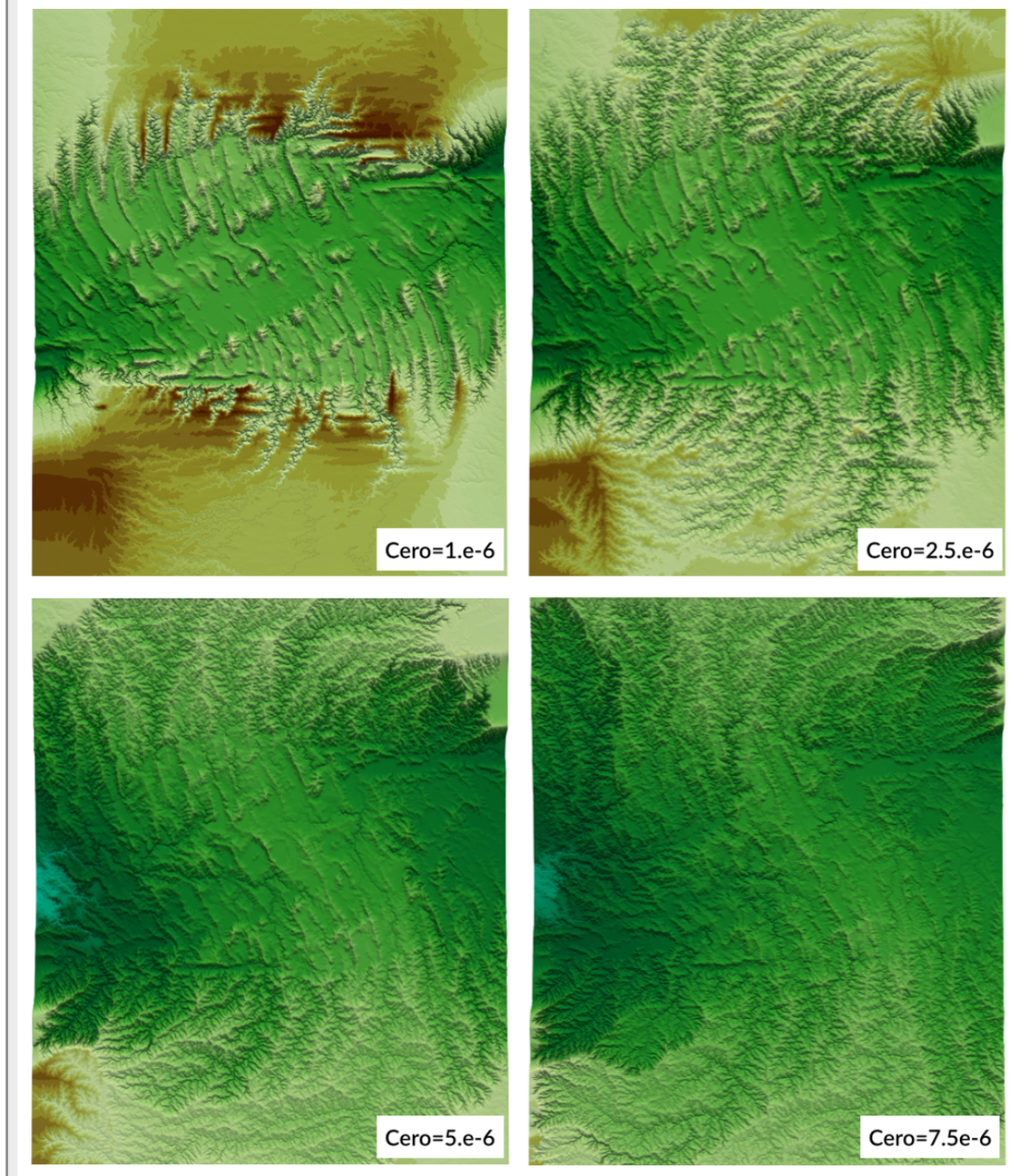

Sensitivity of the landscape to sediment erodibility coefficients.

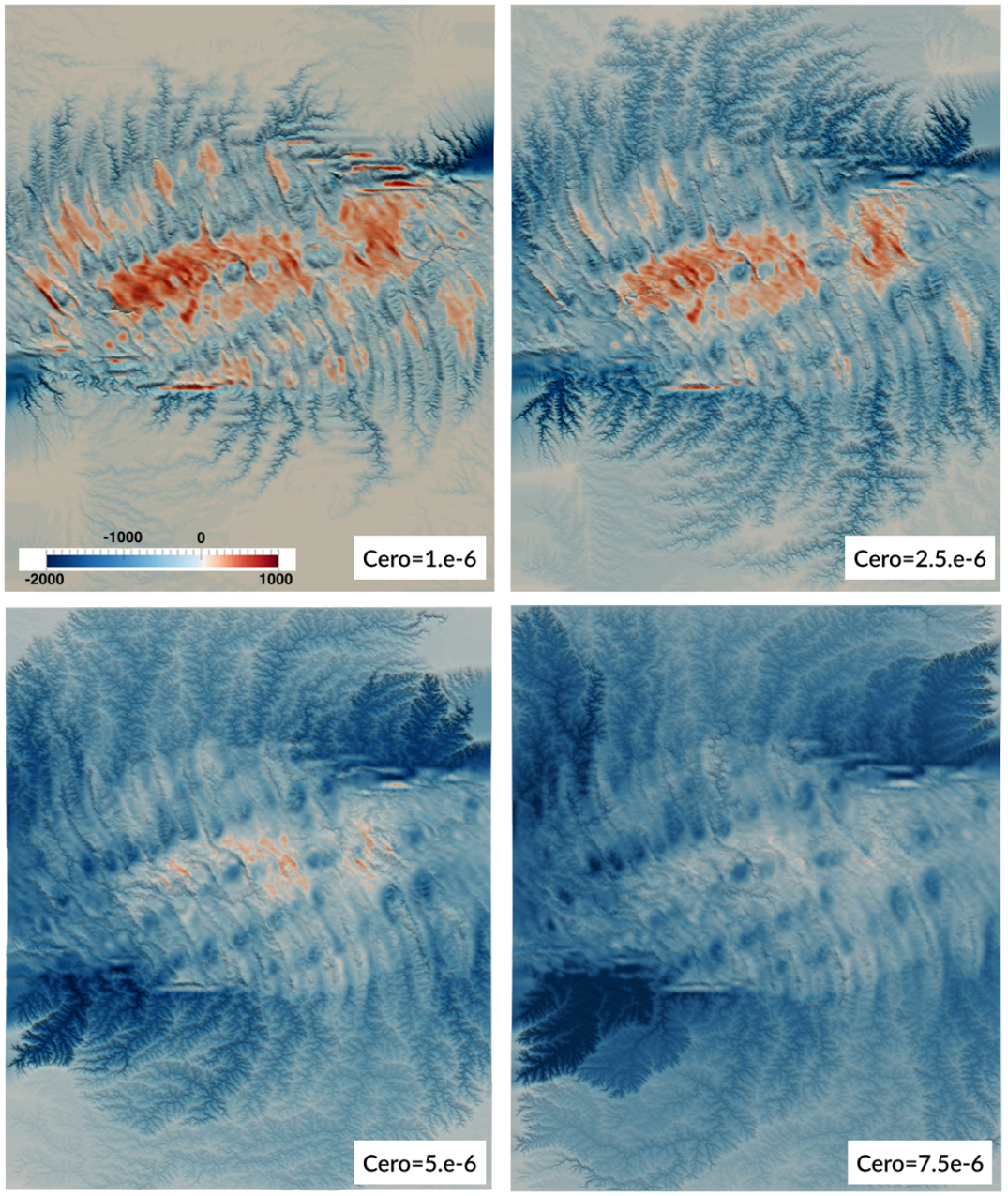

Cumulative erosional/depositional evolution for the different erodibility coefficients.

Basins evolution

The internal structure of these basins is highly variable both in space and time owing to complex stress fields and heterogeneous crustal rheology around the termination of the delimiting faults. This complexity has led to several unresolved problems regarding the kinematics and dynamics of pull-apart basins. Using the coupling between Badlands and Underworld it is now possible to test the time-dependent deformation patterns within pull-apart basins, and the relation of these basins with the adjacent deformed structural domains.

SECTION 6

Landscape evolution at continental scale

KEY POINTS

1. Deep Earth & surface evolution.
2. Basin filling.
3. Deposit preservation.

DEEP EARTH AND SURFACE EVOLUTION

Flow within the deep Earth shapes its surface over tens of million years and thousands of kilometers, with consequences for the evolution of continental-scale topography, drainage patterns and sediment deposition.

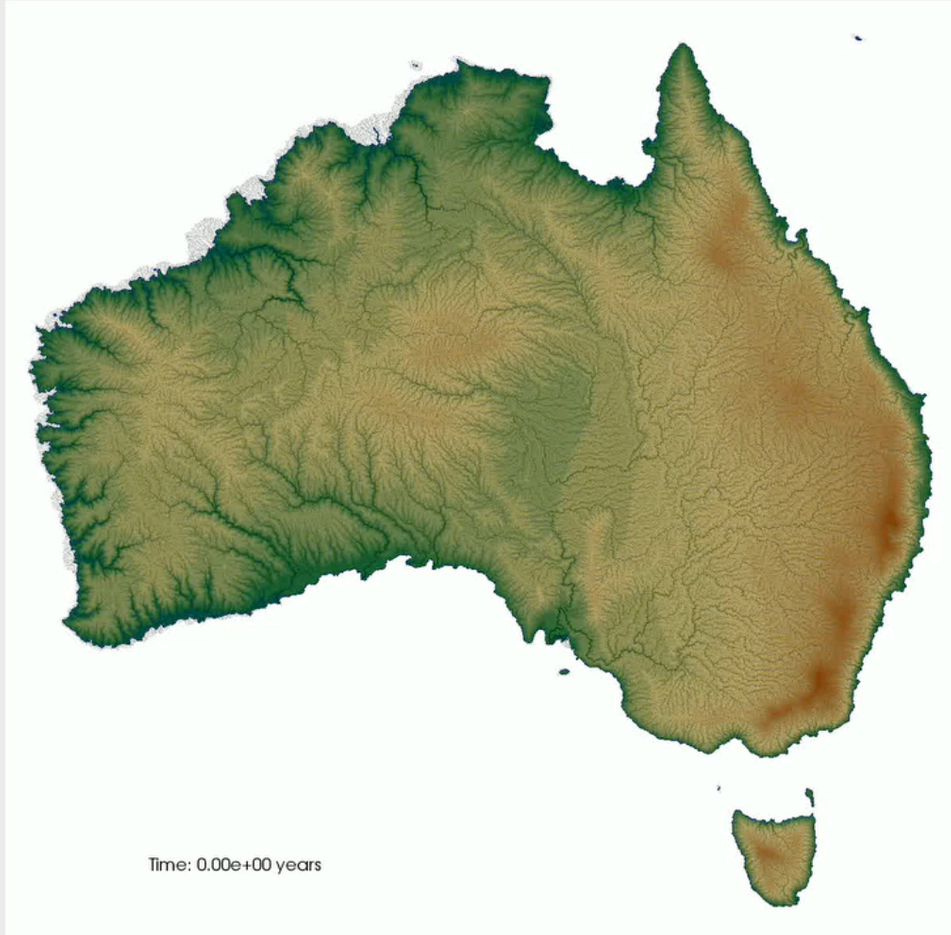

150M years of Australian landscape evolution under dynamic topography, sea-level fluctuations and rainfall variations.

In this example, we investigate the interaction of solid-Earth and surface processes by coupling global tectonic reconstructions and computations of mantle flow (from CITCOMS) with models of erosion, sediment transport and deposition.

We consider the evolution of eastern Australia since the Late Cretaceous, which is characterized by two phases of modelled uplift (~ 200 m) between 120 Ma and 80 Ma, due to the cessation of long-lived subduction at around 100 Ma, and the fast motion of Australia towards the Pacific superswell between 60 Ma and 20 Ma (~ 200 m). These results are consistent with the uplift history deduced from the analysis of river profiles (Czarnota et al., 2014). We couple these dynamic topography predictions with a continental-scale surface process model that we use to compute 100 Myr of landscape evolution from a history of varying climate, sea level and mantle flow.

Basin filling & deposit preservation

The model predicts the time dependence of erosion and drainage patterns that we compare to the sedimentary record in key basins, paleodrainage from paleogeography and denudation rates. In particular, over 5 km of post-rift sediments were deposited in the Ceduna Basin (the southern margin of Australia) in two main phases starting at ~ 80 Ma and ~ 55 Ma. In order to match the Ceduna Basin sedimentation history, we vary the coefficient of erosion by an order of magnitude and the amplitude (between 200 m and 1,000 m) of an uplift event that affected eastern Australia at 95 Ma and that is not fully captured by the mantle flow model. Recorded basin stratigraphy shows the difference in thickness of preserved sediments for the different cases.

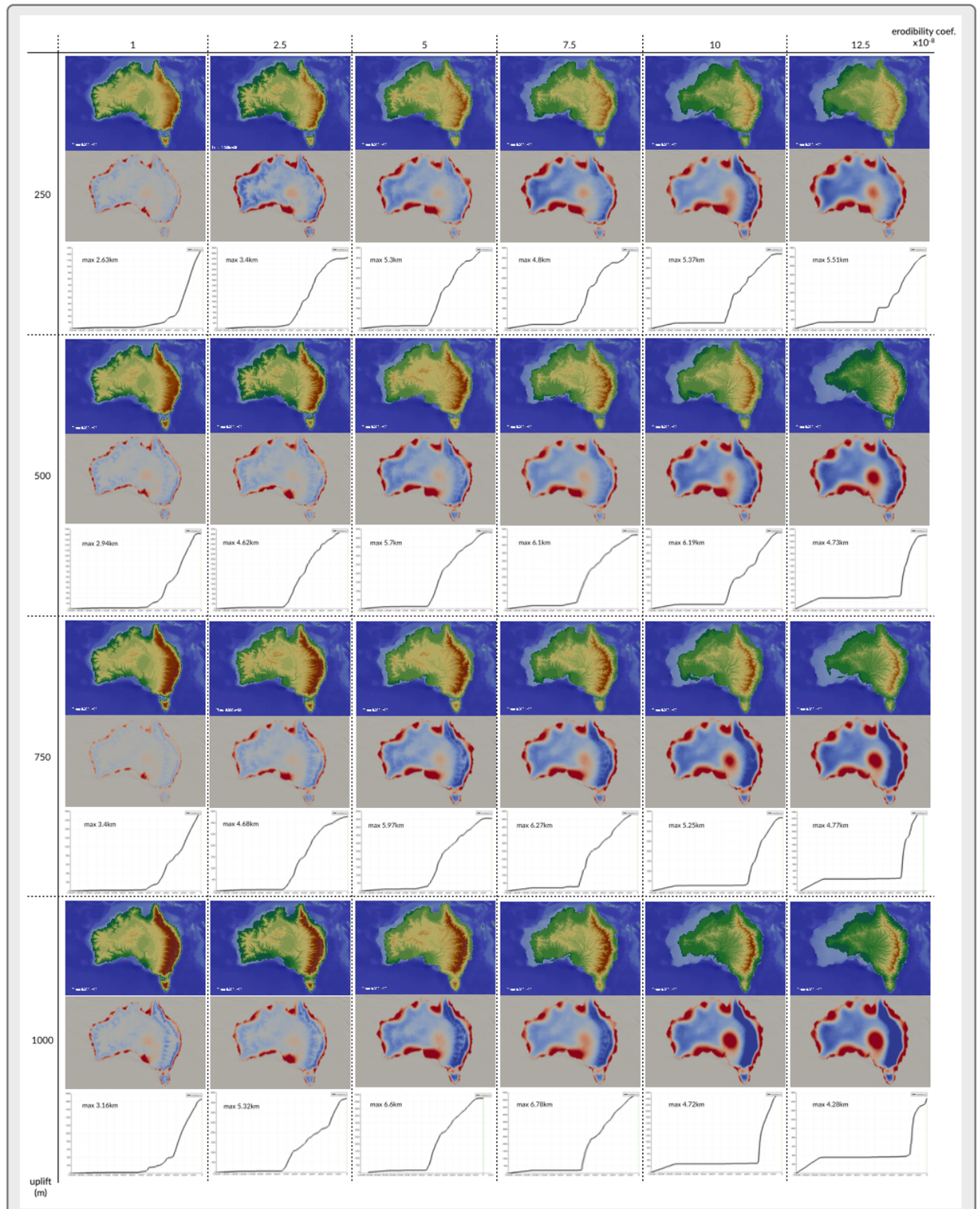

Influence of varying uplift rate and erodibility coefficients on Australian landscape evolution and Ceduna basin deposition. For each set of parameters the figure present 1- final topographic map, 2- cumulative thicknesses after 150 Ma of evolution, 3- averaged deposit evolution for the Ceduna basin region over the 150 Ma (+ maximum thickness in the region).

References

Czarnota, K., Roberts, G. G., White, N. J., Fishwick, S., 2014. Spatial and temporal patterns of Australian dynamic topography from River Profile Modeling, J. Geophys. Res. Solid Earth, 119, 1384–1424.

Flament, N., Salles, T., Müller, R.D., Gurnis, M., 2015. Influence of subduction history and surface processes on continental-scale topography. Abstract for XIV International Workshops on Mantle and Lithosphere Dynamics.